Chapter 1

REVIEW OF STUDIES ON THE DETRIMENTAL EFFECTS OF SOLID CONTAMINANTS IN LUBRICATED MACHINE ELEMENT CONTACTS

George K. Nikas[1]

Imperial College London, Department of Mechanical Engineering,
Tribology Group; London, UK.

Abstract

Maximizing the life expectancy of machine elements in relative motion is the ultimate challenge faced by tribology researchers in industry and academia. However, despite the progress in materials science and lubrication methods, a great obstacle remains in achieving this goal, and that is the presence of solid contaminants in lubricants. The entrainment of 1-100 μm debris particles in concentrated contacts such as in bearings, gears, cam-followers or seals, is associated with various damage modes such as surface indentation and abrasion, lubricant starvation and scuffing, high frictional heating etc. All of these refer to plastic deformations and are detrimental to the life of the machine elements involved and, obviously, to the life of the machine.

This chapter contains a review of theoretical and experimental studies in the literature on the effects of debris particles in lubricated contacts, exploring the progress made in the last few decades. The studies cover the entrainment, entrapment and passage of debris particles through the contacts, and how this is affected by the operating conditions. Analytical, numerical and experimental studies are discussed in view of understanding the damage mechanisms involved in this process. This helps to improve the designs, depending on application requirements, aiming at minimizing the risks, maximizing life expectancy and, thus, improving engineering reliability in industrial, automotive and aerospace applications.

1. Introduction

Machine reliability is the ultimate goal of tribology researchers and engineers in industry and academia. The challenge of maximizing the life expectancy of machine elements in relative

---

[1] Correspondence address: Dr G. K. Nikas, 3 Princes Mews, Hounslow, Middlesex, TW3 3RF, England

motion such as bearings, gears, seals, cam-followers, CV-joints, etc, involves materials and lubrication science, surface physics, and, naturally, an understanding of phenomena taking place on the micro- and nano-scale. In recent times, numerous theoretical and experimental studies have shown the importance of lubricant cleanliness in achieving the designed life expectancy of machine elements. Unfortunately, despite all precautions, the presence of solid contaminants in lubricating systems is unavoidable. Whether such contaminants are carried to the contact by a lubricant as in the case of transportation cans [1,2], atmospheric air, or because of a deficiency or failure of sealing systems, is unimportant; whether they are generated by wear in a concentrated machine-element contact or in neighbouring contacts is of secondary importance. The fact is that in a normal lubrication system such as that of a passenger car engine, millions of particulates exist at any time during the life cycle of the system.

A large volume of the related literature is dedicated to showing that debris particles of 1-100 μm in size are responsible for a large proportion of machine element failures. This has been brought into the foreground in recent decades mainly for two reasons: (a) because of the improvements in the cleanliness and homogeneity of bearing steels, and (b) because of the tightening of tolerances and reduction of film thicknesses in lubricated contacts to sub-micrometre levels. The former reason resulted in reducing bearing failures from contact fatigue initiated below the surface from material inhomogeneity, which is owed to voids or impurities that concentrate stress and are, normally, the sources of cracks. The latter reason (reduction of the average film thicknesses) made lubricated contacts more susceptible to damage from foreign objects because of the additional stress associated with their passage through the narrower contact gaps.

The effects of debris particles have gained a lot of attention in the literature, particularly after the 1980s. It is interesting to note that as far in the past as in the 15th century, Leonardo da Vinci [3] described the wear of metal water wheel axles by wear chips embedded in the wooden supporting bush, as reported by Dwyer-Joyce et al [4]. In machine elements such as bearings and gears operating with a combination of rolling and sliding motion, typical contact gap sizes range from zero in dry contacts to a few micrometres in hydrodynamic contacts. In the majority of cases, as for example in oil lubricated rolling bearings, the film thickness is typically in the order of 0.1 to 1.0 μm. Considering the average size of typical debris particles, which is in the order of 1-100 μm, it is obvious that their entrapment and subsequent squeezing in concentrated contacts can cause significant damage. In hard machine element contacts, as in the majority of cases, particle compression causes substantial stressing in the vicinity of the compressed particle. Depending on the size, hardness and fracture toughness of a particle, the hardness and friction coefficients of the contact counterfaces, as well as the type of motion of the concentrated contact (rolling, sliding, spinning) and the magnitude of the counterface velocities, various damage modes can be distinguished.

In sliding contacts and with particles harder than at least one of the counterfaces, surface abrasion is to be expected [4-12]. In the majority of contacts, regardless of motion pattern and particle hardness, brittleness or morphology, surface indentation is the most common effect [13-16]. This has been studied experimentally as for example in references [15,16] as well as theoretically, either via a simple stress analysis [13,14] or via a Finite Element Analysis [17,18]. Metallic debris particles have also been proved responsible for scuffing failure of contacts [19-29] via two basic mechanisms: (a) by obstructing the lubricant replenishment of

a contact [20,22,25,26], and (b) by generating frictional heat when sheared between the relatively moving counterfaces of a contact [19,21,23-29], which is particularly evident in sliding contacts. The extent of such contact failures could be large as in gross scuffing (or galling) [19,22,24,26] or localised. In the latter case, isolated particles squashed and sheared in narrow contact gaps cause frictional heating that can be quite severe (for example, hundreds of degrees Celsius) [21,23,25, 27-29]. It is notable that this can happen not only for particles harder than the contact counterfaces [19,21,24] but softer, too [23,25,27-29], depending on the contact gap thickness and surface speeds.

Having examined and understood the basic mechanisms of surface damage from debris particles, the next logical step is to study the effects of the induced damage on the life expectancy of machine elements. Numerous such studies exist in the literature and are based on carefully executed, tedious experiments as in references [30-42] or on often complex mathematical analyses as in references [43-46]. There are also a few review studies on debris particle modelling, experimentation and effects, which are of particular value [25,47-51].

Although the emphasis of this chapter is on the detrimental effects of debris particles, there are applications where the intentional use of particles, usually of very small size, has proved beneficial in the lubrication of machine elements. These are not discussed in this chapter the main focus of which is to discuss the mechanisms of debris-induced damage and to present solutions to minimize the related risks.

2. Sources of Solid Contaminants

Generally, the sources of solid contamination can be either internal or external. Specifically, the following categories are distinguished.

2.1. Internal or Built-in

This involves particles remaining after manufacturing and assembly processes. It is an unfortunate fact that new lubricants contain a large number of debris particles. Kjer [1] in 1980 reported the presence of a large number of metallic and non-metallic particles in new motor oils analysed by a ferrographic technique. The particles were of three types:

- spherical particles of a few micrometres and up to 30 μm in size (Figure 1(a));
- metallic wear particles of up to 50 μm in size (Figure 1(b));
- irregular, non-metallic particles of up to 100 μm in size (Figure 1(c)).

(a) Metallic   (b) Metallic, wear   (c) Non-metallic, irregular
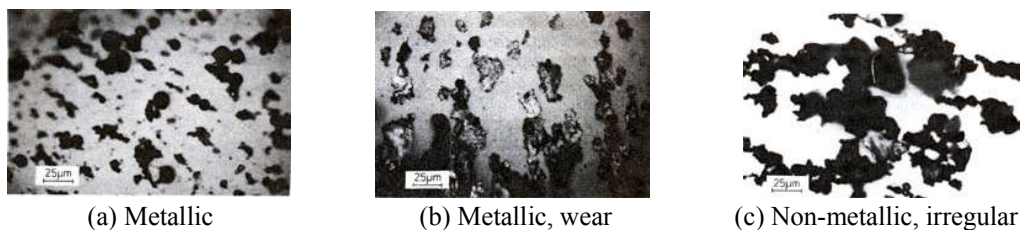
Figure 1. Debris particles in new motor oils (from Kjer [1]).

Leng and Davies [2] in 1988 used both analytical ferrography and spectrometric oil analysis of unused oils produced and canned in South Africa for diesel engines. They observed debris similar to those reported in Kjer [1]. Specifically, they detected (among others):

- calcium-rich mineral particles of up to 30 μm in size, which were the most common contaminants (Figure 2(a));
- silicon-rich mineral particles of up to 25 μm in size (Figure 2(b));
- cutting wear debris (Figure 2(c));
- spherical, iron-based debris, 3-20 μm in size, known to be produced by manufacturing processes such as grinding (Figure 2(d));
- other particles such as particles made of pure chromium (Figure 2(e)) and large organic debris (Figure 2(f)).

(a) Calcium-rich, mineral   (b) Silicon-rich mineral   (c) Cutting wear debris

(d) Spherical, iron-based   (e) Pure chromium   (f) Large, organic
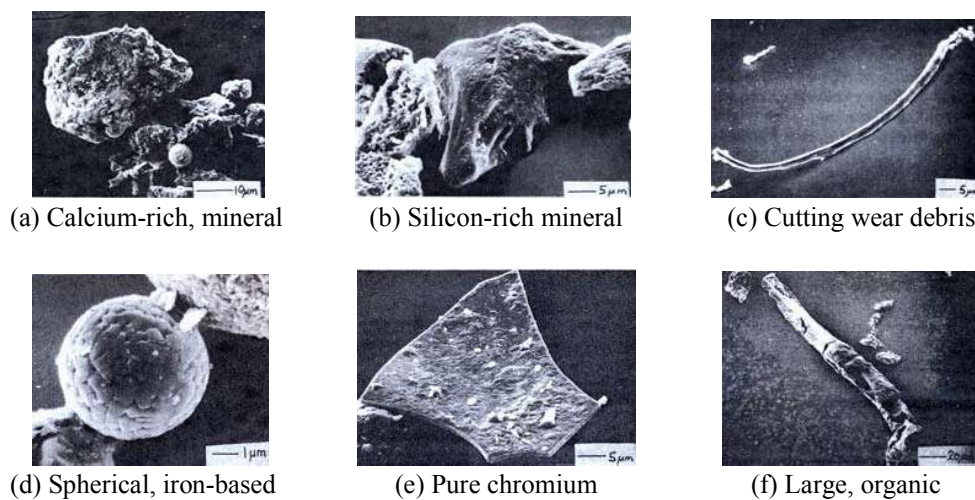
Figure 2. Debris particles in unused lubricants for Diesel engines (from Leng and Davies [2]).

All new oils contain solid contaminants in various concentrations and sizes. In 1991, according to the largest bearing manufacturer, SKF [52], a drum of new oil (about 200 litres) contained more than 1.1 billion particles larger than 5 μm. This is equivalent to 5.5 million particles larger than 5 μm per litre of oil. Dwyer-Joyce [51] in 2005 stated that contamination levels in industrial oil supplies vary from around 0.1 to 10 g/l. Particle sizes vary from sub-micrometre level to 1000 μm [35].

2.2. Generated or Wear Particles

This involves particles generated within a system during operation due to various wear processes such as abrasion (roughness asperities or debris particles ploughing material from a surface), adhesion (particles detached from a surface), erosion, contact and pitting fatigue, spalling, scuffing, etc. Internally generated particles can be the product of combustion such as

soot in diesel engines, metal chips from machining, core sand from castings, paint flakes, rust etc [53]. Such contaminants can be very large, for example, a few millimetres in size.

2.3. Ingested or External

This involves particles entering a system from its environment due to insufficient sealing. Examples include dust and sand particles carried by atmospheric air, railway track ballast, rust, swarf, grits from grinding operations, chips from welds, etc. Such contaminants can also be very large, up to a few millimetres in size.

2.4. Introduced during Maintenance

This involves particles entering a system during maintenance, for example, when changing lubricants or replacing components such as filters, seals etc. The particles introduced this way, obviously, vary a lot in size, morphology and composition.

3. Types of Debris Particles

There are various factors used in the characterisation of debris particles for classification and condition monitoring purposes. A systematic approach includes parameters such as shape, size, surface texture, and material. The literature contains many studies in this respect and only a brief review is presented here. The main goal of such studies is to develop automatic classification methods for wear particles in order to monitor the condition of machine parts such as bearings, gears, seals, etc, and decide whether maintenance or repair is due. It has been realised in recent decades that this approach is invaluable for preventative maintenance as well as for establishing potential causes of machine element deterioration or failure [54, 55].

One of the main factors in particle characterisation is "morphology". This refers to particle appearance, which is a rather vague term, yet still useful for a qualitative description. For example, Roylance et al. [56] provide the classification similar to that shown in Figure 3. Trevor [57] distinguishes the following categories in reference to particle morphology, as reported by Kowandy et al. [58]:

- spheres;
- distorted smooth ovoids;
- chunks and slabs;
- platelets and flakes;
- curls, spirals and slivers;
- rolls;
- strands and fibres.
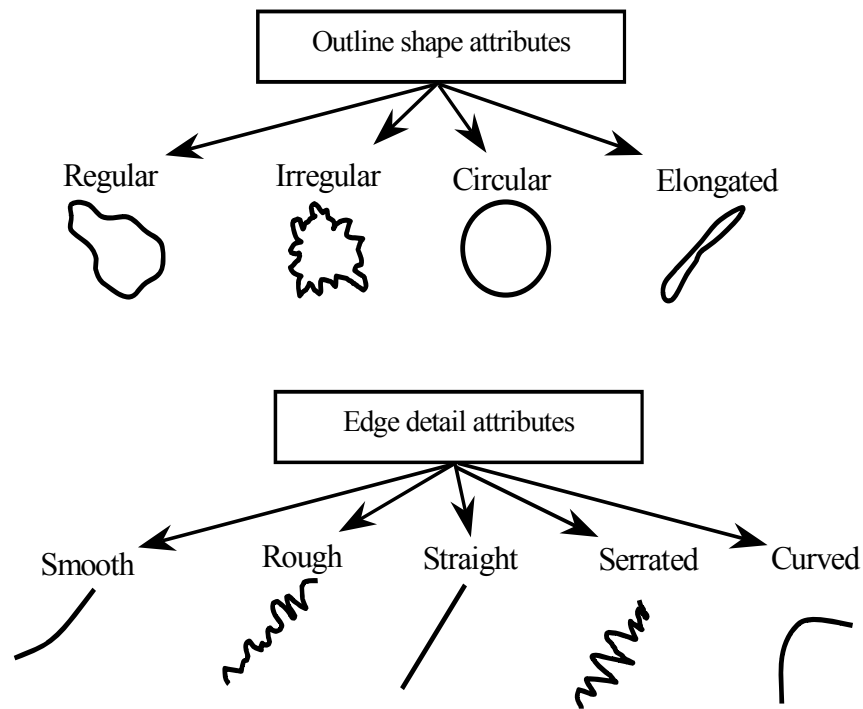
Figure 3. Particle outline-shape and edge-detail attributes (adapted from Roylance et al. [56]).

In general, principal morphological attributes of wear particles used in establishing the wear process creating the particles are size, shape, surface topography, colour and thickness [59]. Scanning Electron Microscopy (SEM) is normally used for the visual examination of particles but such a visual method requires expert knowledge and is time-consuming, costly and often inconsistent. Therefore, a set of numerical descriptors and protocols had to be developed in order to computerize the classification process, making it faster, more consistent and more formal. Such numerical descriptors involve particle size (apparent area, length, perimeter, equivalent-circle diameter) and outline shape [60] (aspect ratio, shape factor, convexity, elongation, curl, roundness, etc). For further information, the reader is referred to references [56, 57, 61-63] and the references quoted therein.

Image analysis systems for wear particles have been developed by several researchers. Stachowiak and co-workers, taking into account the fractal topography of particles, have developed fractal particle-boundary descriptors. Interested readers are referred to Stachowiak [60] and the references quoted therein. The benefit of such techniques is that the destructiveness of particles (for example, their abrasivity) can be quantified when other properties are known, as for example their hardness.

One of several interesting classifications in terms of particle shape that are available in the literature can be found in Trevor [57] and is shown in table 1. This is helpful in a preliminary and quick identification of possible origins of the detected particles based on their shape.

Table 1. Shapes of particles and their possible origins
(from Trevor [57] as reproduced by Kowandy et al. [58]).

Particle shape	Typical names	Some possible origins
	Spheres	Metal fatigue
	Distorted smooth ovoids	Quarry dusty; atmosphere dust
	Chunks and slabs	Metal fatigue; bearing petting; rock debris
	Platelets and flakes	Running-in metal wear; paint; copper in grease
	Curls, spirals and slivers	Machining debris produced at high temperature
	Rolls	Probably similar to platelets but in a rolled form
	Strands and fibres	Polymers, cotton and wood fibres; occasionally metal

Another interesting classification was presented in Bowen and Westcott [64] and Anderson [65]. This is presented in table 2, as reproduced by Roylance et al. [59].

Table 2. Wear particle morphological descriptors. Sizes stated apply to particles obtained from oil or grease samples (from Bowen and Westcott [64] and Anderson [65], as reproduced by Roylance et al. [59]).

Particle type	Description
Rubbing	Particles < 20 μm chord dimension and approximately 1 μm thick. Results from flaking of pieces from the shear-mixed layer.
Cutting	Swarf-like chips of fine wire coils. Caused by abrasive "cutting-tool" action.
Laminar	Thin, bright, free metal particles, typically 1 μm thick, 20-50 μm chord width, with holes in surface and uneven edge profile; emanates from mainly gear and rolling element bearing wear, associated with fatigue action.
Fatigue	Chunky, several micrometres thick; for example, 20-50 μm chord width.
Spheres	Typically ferrous, 1-50 μm diameter; generated from microcracks; generated under rolling contact conditions.
Severe sliding	Large, 50 μm chord width, several micrometres thick. Surface heavily striated with long straight edges. Typically occurs in gear wear.

If the operating and environmental conditions in a machine are known, it does not require a lot of experience to recognise some characteristic wear debris and the associated wear process that created them. For example, wear debris with a ribbon-like form of machined swarf are characteristic of severe abrasion of a softer surface by a hard, rough counterface (abrasion by roughness asperities); they are also characteristic of a sliding contact contaminated by hard particles with sharp edges [59]. Contact fatigue processes on the other hand tend to produce relatively large wear particles of blocky, irregular shape [59] (see also table 1 and 2); spherical metallic particles are also characteristic of machining processes such as grinding – see for example Figure 2(d). However, caution should be exercised even with automatic pattern-recognition systems because classification errors cannot be ruled out when relying on particle morphology alone. For example different adhesive wear conditions can produce similarly looking particles [66]. Therefore, other factors should be accounted for in order to improve detection accuracy and fault diagnosis.

The material of debris particles is established with various methods such as ferrography [54], energy dispersive spectroscopy, IR and X-ray emission analysis. Materials often found in debris particles from lubricant samples include iron (Fe), aluminium (Al), silver (Ag), copper (Cu), carbon (C), zinc (Zn), tin (Tn), silicon carbide (SiC), silica, lead (Pb), chromium (Cr), calcium (Ca), phosphorus (P), and sulphur (S). The last three of those and zinc can also be attributed to lubricant additives. Table 3 shows an example of the materials and particulate concentrations of various lubricant samples.

Table 3. Debris particles found in lubricant samples from various sources (from Dwyer-Joyce [49]).

Investigator	Sample source	Concentration (estimated) [g/l]	Size range [μm]	Materials present
Dwyer-Joyce [49]	Paper mill	0.4	0-150	Cu, Sn, silicates
Dwyer-Joyce [49]	Motor vehicle sump	1-2	0-250	C, Fe
SKF-ERC (Beghini et al. [67])	Various bearing lubricants	0.3-1.5	0-250	Fe, Al, Cu, Sn, SiC, sand
Admiralty Engineering Laboratory	Various		0-100	Al, Ag, Cr, Zn, Fe
Eleftherakis and Khalil [68]	Motor vehicles	0.3	0-120	Al, Cu, Fe, Pb
Loewenthal and Moyer [31]	Aircraft gas turbines	1-2	0-200	Fe, C, silicates

One of the most important parameters in assessing the risk of damage from debris particles is the particle hardness. A general description can be found in table 4.

Table 4. Types of particles in terms of hardness
(see for example [49,52] and table 6.1 in [69]).

Particle	Hardness [Vickers]	Type	Source
Very soft	Up to 40	Plastics, paper, wood, textile and vegetable fibres, pure metals such as gold, silver, copper, lead, tin, aluminium and nickel	External for the non-metallic materials; external and internal (e.g., oatings) for the metallic materials
Soft, metallic	55-280	Mild steel, brass, bronze, aluminium, copper	Housings, bushings, etc.
Hard, metallic	700 (typical)	Steel (bearings, gears); cast iron	Hardened surfaces
Tough material (but brittle)	Usually up to 1300 for ceramics but could be even more for other materials	Ceramic (silicon carbide, silicon nitride); corundum (aluminium oxide)	Manufacturing (lapping paste, grinding wheels, etc.

In the case of wear particles, the source, naturally, is related to the particular application [49]. For example, worn gears may release steel particles. Worn bushes or housings may release aluminium, bronze and copper. Casting moulds may release silicates (dust, sand). Other particles may be brought in from the environment, for example, dust and sand from the atmospheric air, ceramics such as silicon carbide left over from machining operations (e.g., inding), etc.

Bearing and other machine element manufacturers are aware of the nature of debris expected in any application related to their products and many have internally-produced research results to estimate the risks and suggest the proper level of filtration or lubricant cleanliness. Most of these internal results are confidential and rarely released. Oil cleanliness standards and protocols have been developed to formalise testing procedures and prevent system failures, particularly in critical applications such as those in the aerospace industry. For further information and a brief introduction, the reader is referred to Sasaki [70].

4. Detrimental Effects of Debris Particles in Lubricated Contacts

There is a significant volume of literature devoted to the effect of solid contaminants in machine element contacts. This section begins with general remarks to accustom the reader to the seriousness of this issue and progresses with analysing individual aspects of the problem.

The effects of solid contaminants on hydrodynamic bearing performance were quite early recognised and studied. McKee [71] in 1927 measured an increase in running friction of such bearings. Roach [72] in 1951 and Rylander [73] in 1952 reported on a temperature increase resulting from the increased friction in addition to the increased wear. Similar results were reported by Broeder and Heijnekamp [74] in 1965. Fitzsimmons and Clevenger [75] in 1977 found that the wear of tapered roller bearings is proportional to the amount of contaminants in

the lubricant. Ronen et al. [32] in 1980 studied the performance of hydrodynamic bearings with contaminated lubricant. Their test bearing rig simulated an automotive, connecting-rod, engine bearing. Their results showed that both shaft and liner wear increased, typically, by a factor of 20 when running with contaminated oil. Qualitatively similar results were also reported by Ronen and Malkin [76,77].

In 1971, General Motors Corporation (USA) summarized the effects of debris particles on rolling bearing life as follows [49,50,78]: "*The presence of dirt or grit in ball bearings is responsible for over 90% of all bearing failures; where bearings are kept clean during mounting, are lubricated with clean oil and are protected by recommended closures, no difficulty should be experienced from this source.*"

In tests performed by Okamoto et al. [79] in 1974, it was shown that bearing life is reduced by 80 to 90% when ceramic, silica and iron particles are continuously fed to the bearing lubrication system at 12 mg/h. Dalal et al. [80], also in 1974, performed tests, which showed that bearing life is improved several-fold when an ultra-clean lubrication system is used in place of a system with a 10 μm filtration ability. Loewenthal and Moyer [31] in 1979 showed similar results, that is, an increasing bearing life with finer filtration. Loewenthal et al. [33] in 1982 performed fatigue tests on groups of deep-groove ball bearings with two levels of filtration. They concluded that "*ultra-clean lubrication produced bearing fatigue lives that were approximately twice that obtained in previous tests [31] with contaminated oil using 3 μm absolute filtration and approximately three times that obtained with 49 μm filtration*".

In a study published in 1979 by Wedeven [81], it is recognised that debris is a major factor in component failure of aircraft propulsion systems. According to a study by Cunningham and Morgan [82] in 1979, bearing rejection-causes for aircraft engine, transmission and accessory bearings indicates that the solid contaminants are responsible for approximately 20% of all bearing rejections.

In a series of fatigue tests, Bachu [83] in 1980 used wear debris particles generated by a gear machine (see also the report of Sayles and Macpherson [84] and Webster et al. [85]) and varied the filter-element size as follows (sizes in micrometres): 40, 25, 8, 3, 1 and sub-micrometre. The sub-micrometre filter was a magnetic device and the rest were of the standard, porous-media, cartridge type. The results indicated a 7-fold reduction of the L_{10} fatigue life (the life at which 10% of the bearing population is expected to fail) under 40 μm filtration compared with 3 μm filtration, the difference attributed to surface indentations from the larger debris passing through the poorer filter. Moreover, running a group of bearings with a 40 μm filtration for 30 minutes, then changing to the 3 μm filter and continuing the test to the remaining of the life of the bearings gave very similar L_{10} fatigue life to that obtained with 40 μm continuous filtration. This indicates that early surface damage from debris defined the ultimate fatigue life and that subsequent, continued presence of debris in the bearings had little effect on fatigue life. In other words, fine filtration during the running-in period of a lubricated system is critical for its life expectancy. In tests performed by Nilsson et al. [42] in 2005, it was found that "*filtration during run-in for one hour with a 3 μm filter can reduce both the mass loss and the number of self-generated particles by a factor of 10*". This is a well-known fact nowadays to, for example, car engine manufacturers who recommend flushing the lubricating system of a new engine after a very short period of time (a few hundred kilometres maximum), as opposed to future oil services.

In 1991, the largest bearing manufacturer, SKF, categorized the causes of bearing replacement as follows [52]: 36% were owed to poor lubrication, 34% were owed to normal fatigue, 16% were owed to incorrect installation, and 14% were owed to contamination failure.

According to Ai [41] (The Timken Company, USA) in 2001, it has been estimated that 75% of bearings that failed before reaching their rated lives have failed from contamination. Naturally, such percentages vary a lot between manufacturers and end users depending on how meticulously lubrication systems are serviced and how efficient the filtration is. In this author's opinion, such figures cannot be taken as gospel but as indicative of how easy it is to cause damage to machine components if attention is not paid to proper filtration and removal of harmful solid contaminants.

The role of proper filtration, as already emphasized, is major in reducing machine element wear from debris particles and avoiding premature failures. Given the high concentrations of harmful particles in new and used lubricants, as explained in sub-section 2.1, using the correct filter for the particular application is of great importance. A common misunderstanding in this area concerns the efficiency rating of a filter and its real consequences on filtration.

According to ISO Standard 4572, a filter can be rated using the following ratio:

$$\beta_x = \frac{\text{number of particles per volume unit (100 ml) larger than } x \text{ } \mu\text{m upstream the filter}}{\text{number of particles per volume unit (100 ml) larger than } x \text{ } \mu\text{m downstream the filter}} \tag{1}$$

Obviously, this "beta ratio" rating refers to a specific particle size in micrometres, indicated by subscript x in β_x. For example, a filter rating of $\beta_{14} = 200$ means that for every 200 particles of size 14 μm ($x = 14$) upstream the filter, only one particle is expected to pass all the way through the filter. This is clear to comprehend and take into consideration. However, what is most often quoted commercially is the filtration efficiency, η (as a percentage [%]), which is defined as follows:

$$\eta = \frac{\text{number of retained particles}}{\text{number of inlet particles}} = 100 - \frac{100}{\beta} \tag{2}$$

For example, the filtration efficiency for the previously quoted example of $\beta_{14} = 200$ is $\eta = 99.5\%$ for 14 μm particles. This may sound sufficient to someone, who might assume that an efficiency of 99.9% in this case is not much better or not really necessary. However, using $\eta = 99.9\%$ and solving for beta from Eq. (2), the result is $\beta_{14} = 1000$, which is five times better (or, equivalently, five times cleaner lubricant) than the original rating $\beta_{14} = 200$. In general, using Eq. (2), it is easily proved that a filter with 99.9% efficiency is ten times more effective than a filter with 99% efficiency. For this reason, caution must be applied when considering efficiency ratings because, as demonstrated with the previous examples, small percentage changes can disguise the extent of lubricant contamination.

The level of lubricant contamination and filtration efficiency has been incorporated in bearing life calculations in an attempt to improve the accuracy of bearing life predictions. Ball bearing manufacturer SKF and its New Life Theory for example uses an adjustment

factor for bearing life rating, which is a function of (among others) a factor η_c for "contamination level" (see page 62 in reference [86]). The calculation of this factor is based on ISO standards for classification of the contamination level in lubrication systems (ISO 4406:1999) as well as on the viscosity ratio κ (in SKF's terminology) and the size of a bearing – see reference [86] for full details. General guidelines for estimating η_c do exist (see for example table 4 on page 62 of reference [86]), giving value ranges of η_c in cleanliness conditions characterised with adjectives shown in table 5.

Table 5. Guideline values for oil contamination factor η_c from SKF's General Catalogue [86].

Lubricant condition	Description
Extreme cleanliness	Particle size of the order of the lubricant film thickness. Laboratory conditions.
High cleanliness	Oil filtered through extremely fine filter. Conditions typical of bearings greased for life and sealed.
Normal cleanliness	Oil filtered through fine filter. Conditions typical of bearings greased for life and shielded.
Slight contamination	Slight contamination in lubricant.
Typical contamination	Conditions typical of bearings without integral seals, coarse filtering, wear particles and ingress from surroundings.
Severe contamination	Bearing environment heavily contaminated and bearing arrangement with inadequate sealing.
Very severe contamination	Severe reduction of bearing life ($\eta_c = 0$)!

A characteristic example of the effect of lubricant contamination on bearing fatigue life is provided on page 64 of SKF's General Catalogue [86] stating the following: "*Several 6305 deep groove ball bearings with and without seals were tested in a highly contaminated environment (a gearbox with a considerable number of wear particles). No failures of the sealed bearings occurred and the tests were discontinued for practical reasons after the sealed bearings had run for periods which were at least 30 times longer than the experimental lives of the unsealed bearings. The unsealed bearing lives equalled 0.1 of the calculated L_{10} life, which corresponds to a factor $\eta_c = 0$.*"

(a) New oil   (b) Contaminated oil
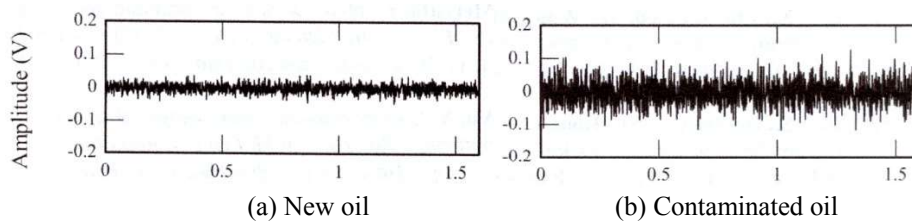
Figure 4. Vibration waveforms after 60 minutes for new oil (left) and oil contaminated with 40 μm particles (right). The horizontal axis refers to the running time in seconds. (From Akagaki et al. [87].)
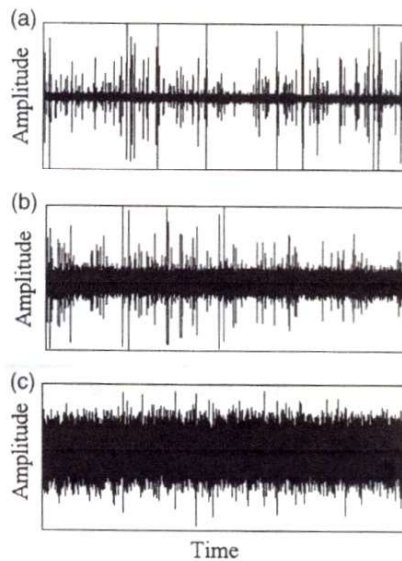
Figure 5. Amplitude of the acoustic emission time signal with three contaminated greases: (a) grease with 0.02% by weight of quartz dust; (b) grease with 0.2% by weight of quartz dust; (c) grease with 2% by weight of quartz dust.

Bearing deterioration following lubricant contamination can be detected acoustically through vibration analysis equipment. Figure 4 shows some of the results of Akagaki et al. [87] on the vibration waveform tests done on new oil and oil contaminated with 40 μm particles. The difference is obvious. Miettinen and Anderson [88] showed similar results for rolling bearings lubricated with contaminated grease (Figure 5).

The effects of lubricant solid contaminants are of course not confined to rolling bearings, although they are better known in this sector because of the fine tolerances, thin lubricating films and wide range of applications in industry and transport. Other machine elements such as gears and seals deteriorate when operating in contaminated environments. For example, Sari et al. [89] showed the degradation of spur gears operating with lubricant contaminated with very fine sand particles, in an attempt to simulate operating conditions such as those met in deserts, quarries or mines. They showed that the particles increase the abrasive wear and surface temperature in zones of high sliding, particularly at the teeth roots. Furthermore, the effects of debris are not confined to wear. Mizuhara et al. [90] used a two-disc rig operating in the mixed to hydrodynamic lubrication regime and contaminated the lubricant with spherical, very hard alumina particles. Thus, they showed that friction increased with particle concentration but the effect was diminished at higher sliding velocities, probably due to the thicker hydrodynamic film, which offset the load supported by the particles. They later extended their study with a theoretical analysis of the effects of particles on the friction of journal bearings [91].

5. Particle Behaviour and Mechanisms of Damage to Lubricated Contacts

Particle behaviour in lubricated contacts depends on the size, hardness and fracture toughness of the particles. It also depends on the hardness of the contact counterfaces and on the kinematical conditions of the contact. Extensive experimental studies and theoretical analyses since the 1980s have shown that, in terms of particle material properties, the following four categories can be classified [49,50] (all referring to isolated particles in, predominantly, rolling contacts).

(a) Ductile particles passing through a concentrated contact are flattened and become thin platelets with a thickness approximately equal to the average film thickness of the contact. If plastic deformation of the contact counterfaces takes place, the flattened particles appear more like "flying saucer discs" – see Figure 6(a).

(b) Brittle particles fracture early in the inlet zone and produce small fragments that imbed surfaces – see Figure 6(b). Surface damage depends on the ultimate fragment size in relation to the film thickness of the contact.

(c) Tough particles may fracture late in the inlet zone producing large fragments that imbed surfaces – see Figure 6(c). The fragments are generally larger than in the case of weaker, brittle particles (case (b)) and the immediate damage to the surfaces will be greater.

(d) Small, tough particles behave rigidly – see Figure 6(d). If they are larger than the average film thickness of the contact, the contact counterfaces are forced to deform elastically or plastically to accommodate them.
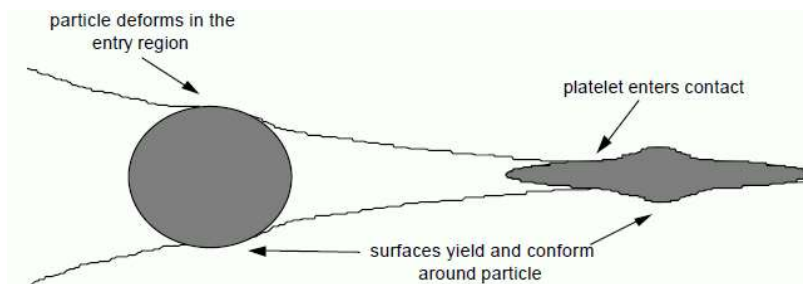
(a) Ductile particles are flattened and become thin platelets.
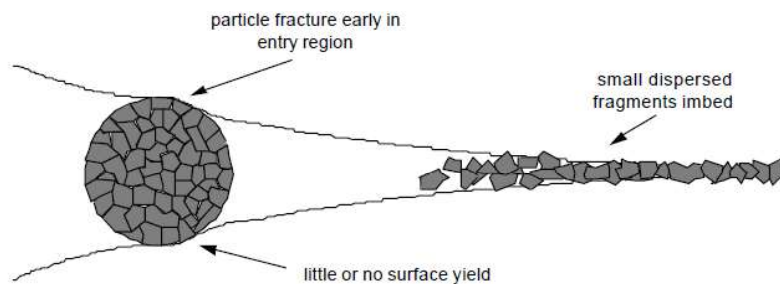
(b) Brittle particles fracture early in the inlet zone producing small fragments that imbed surfaces.

Figure 6. Continued on next page.

(c) Tough particles fracture late in the inlet zone producing large fragments that imbed surfaces.

(d) Small, tough particles behave rigidly.
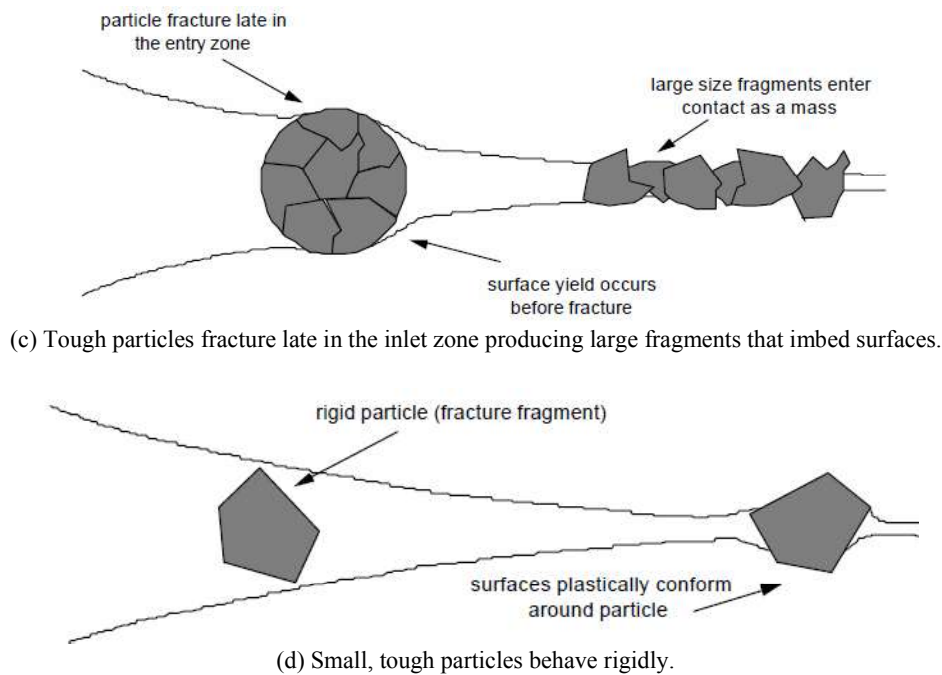
Figure 6. Behaviour of particles in rolling contacts depending on particle material properties (from references [49,50]).

5.1. Soft, Ductile Particles

Ductile particles entering an elastohydrodynamic contact with average film thickness smaller than the average particle size will be elastoplastically deformed [15,16,35,49]. Depending on the particle hardness in relation to the contact surface hardness, a particle may or may not cause plastic deformation to the contact counterfaces. If the particle is relatively soft, it will be extruded as it is being squashed between the harder counterfaces of the contact. This extrusion involves some sliding between the particle and the contact counterfaces as well as some sticking, depending on the local friction coefficients. Interfacial friction increases the pressure between the particle and the counterfaces. Depending on the size and hardness of the particle, the counterface deformation may be elastic or elastoplastic. In some cases, the counterfaces can close around the particle before damage (yielding) occurs. Otherwise, plastic deformation in the form of counterface indentation takes place. The process is depicted in Figure 7.

In the 1980s, Hamer et al. [13,14] developed an effective analytical model to calculate the contact pressure on a ductile particle and the displacements of the (flat) counterfaces, assuming the particle is a circular disc and the counterfaces are flat. The particle was extruded as a fully plastic solid squeezed between elastic counterfaces. The analysis was axisymmetric and included friction at the particle-counterface interfaces. The model was capable of predicting the onset of surface yield and was subsequently used to construct maps detailing safe and unsafe regions of operation, such as the one shown in Figure 8. It was later extended to calculate the contact pressure from Johnson's plastic cavity model [92] and, finally, from a Finite Element Analysis in order to account for plastic deformations of the counterfaces [93].
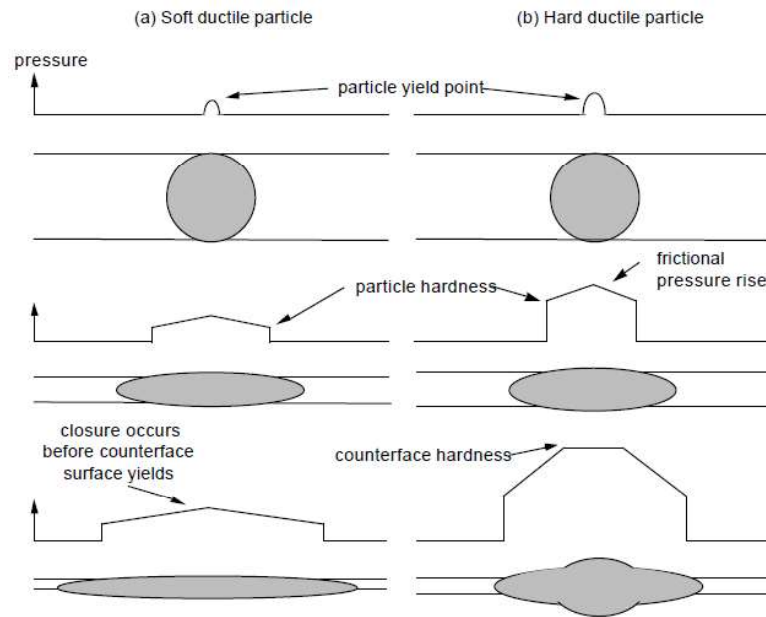
Figure 7. Mechanisms of indentation by (a) soft, ductile particle and (b) hard, ductile particle (from Dwyer-Joyce [49]).
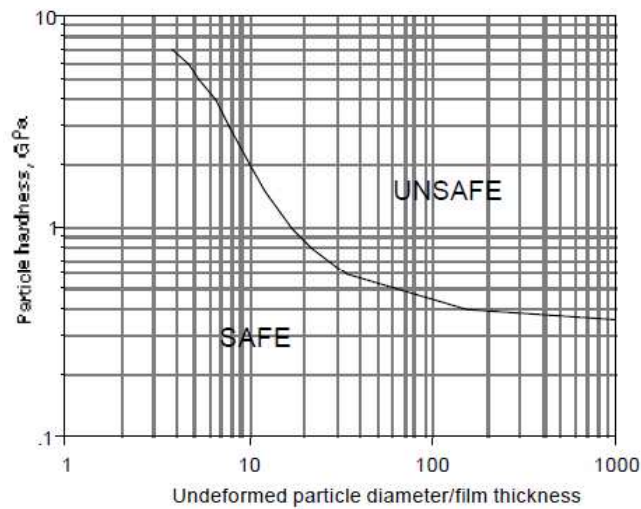
Figure 8. Safe and unsafe combinations of particle hardness and particle diameter to film thickness ratio (from the work of Hamer and Hutchinson [93]).

A basic rig was constructed to study the deformation of soft, ductile particles squashed between hard anvils, and the development of surface indentations [14,93]. Figure 9 shows a schematic of the rig and some characteristic dents, revealing how softer particles produce wider and shallower dents, and how even a 55 HV aluminium solid can indent a 1010 HV surface (Figure 9(d) – bottom, right).
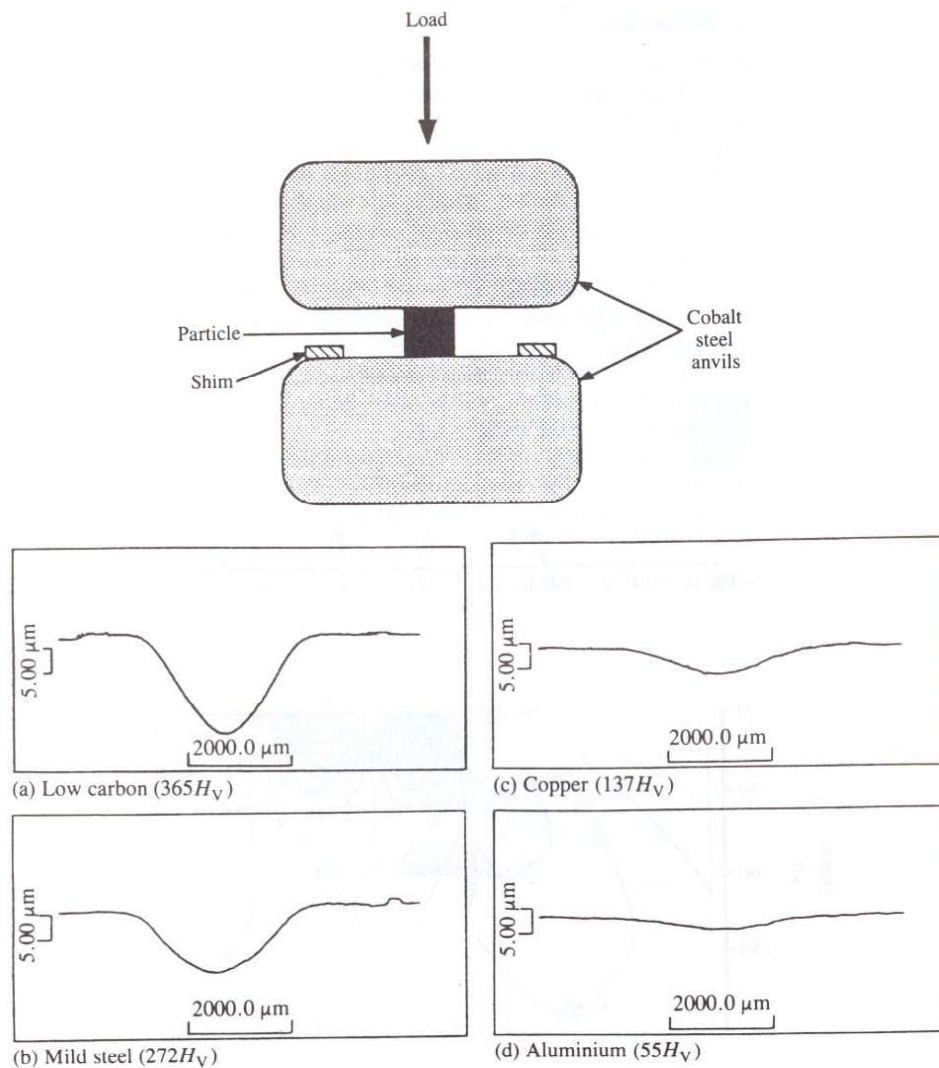
Figure 9. Schematic of particle squashing rig (top) and surface indentations (bottom) when thin discs of volume equivalent to 1.5 mm diameter spheres are compressed to closure between lubricated anvils of hardness equal to 1010 HV (from the work of Hamer and Hutchinson [14,93]).

The predictions of the model by Hamer et al. [14,93] agreed reasonably well with experimental results on the shape of surface indentations, although there was discrepancy in terms of dent dimensions, which was speculated that could be reduced if plasticity effects such as strain hardening were included in the model. For a comparison of experimental results and theoretical calculations, the reader is directed to table 3.6 of Dwyer-Joyce's thesis [49]. The contact pressures were also as expected, with the characteristic "friction hill" as in forging. Figure 10 shows examples of the theoretical predictions on the contact pressure when the contact counterfaces are assumed purely elastic as well as when Johnson's cavity model is utilised to model surface plasticity.

The analysis of Hamer et al. [14] lead to the development of a simple equation to predict the critical parameter values during ductile particle squashing that will cause surface plastic deformation. This is expressed as follows [48]:

$$\frac{D}{t} = \frac{1}{\mu}\ln\left(2\sqrt{3}\,\frac{H_s}{H_p}\right) \tag{3}$$

where D is the effective diameter of the flattened particle, t is the thickness of the flattened particle, μ is the friction coefficient at the interface between the particle and the contact counterfaces, H_s is the hardness of a counterface, and H_p is the hardness of the particle. Critical particle aspect ratios D/t can thus be calculated from Eq. (3) and maps of safe and unsafe regions of operation can be drawn, such as those presented by Sayles et al. [48]. This analysis is less accurate for higher aspect ratios. Nevertheless, it has drawn the important conclusion that in most bearing applications, particles softer than about 40 HV can be regarded harmless in rolling contacts with typical elastohydrodynamic film thicknesses. However, the situation is different when there is sliding in the contact, as is explained later.

As already mentioned, Hamer and Hutchinson [93] used Finite Element Analysis (FEA) to advance the original analytical model of Hamer et al. [13] with plasticity effects (in addition to using Johnson's cavity model). FEA was also used by Dwyer-Joyce [49]. In the 1980s, Ko and Ioannides [17] used FEA to find the dent shapes and sizes from the squashing of ductile debris between flat surfaces. They developed an axisymmetric model (contact of a sphere on a flat surface) and a plane-strain model (contact of a cylinder on a flat surface). However, instead of solving the complete, three-body extrusion problem, they derived the contact pressure from the work of Hamer et al. [13,14] and applied it directly to one of the surfaces (platens). Their calculated dent shapes were found to be in good agreement with experimentally measured dent shapes. FEA on debris indentation modelling has also been used by Xu et al. [43] but only as a simplification via a rigid spherical indenter. Nevertheless, dent profiles were in reasonable agreement with experimental results. More recently, basic debris indentation modelling has been performed by Kang et al. [18] and Antaluca and Nélias [94].

In the 1990s, Nikas [25] took over the debris modelling work at Imperial College London, following up on the analyses of Hamer, Dwyer-Joyce, Sayles and Ioannides. His work involved the elastoplastic modelling of ductile particles, softer than the counterfaces squashing them. He developed numerical models to calculate the contact forces on plastically deforming particles in line, rolling-sliding, elastohydrodynamic contacts, including the fluid forces on the particle from the surrounding lubricant under pressure [23]. He then proceeded to include frictional heat generated between the particle and the contact counterfaces as the particle was extruded in rolling-sliding contacts (for any slide-roll ratio), adding the heat generated inside the particle during its rapid plastic deformation [27]. For that, he modelled a particle as a group of heat sources and utilized the theory of thermoelasticity and moving sources of heat [95-97] to calculate the transient flash temperatures on the contact counterfaces. His results confirmed some earlier results of Khonsari and Wang [21] (further extended in reference [24]) with a much simpler model of hard, abrasive particles that caused high frictional heating and could be deemed responsible for scuffing damage. Some basic

work in this respect has also been presented by Hou and Komanduri [98-100] on the polishing of ceramic balls and rollers in the presence of abrasive particles.
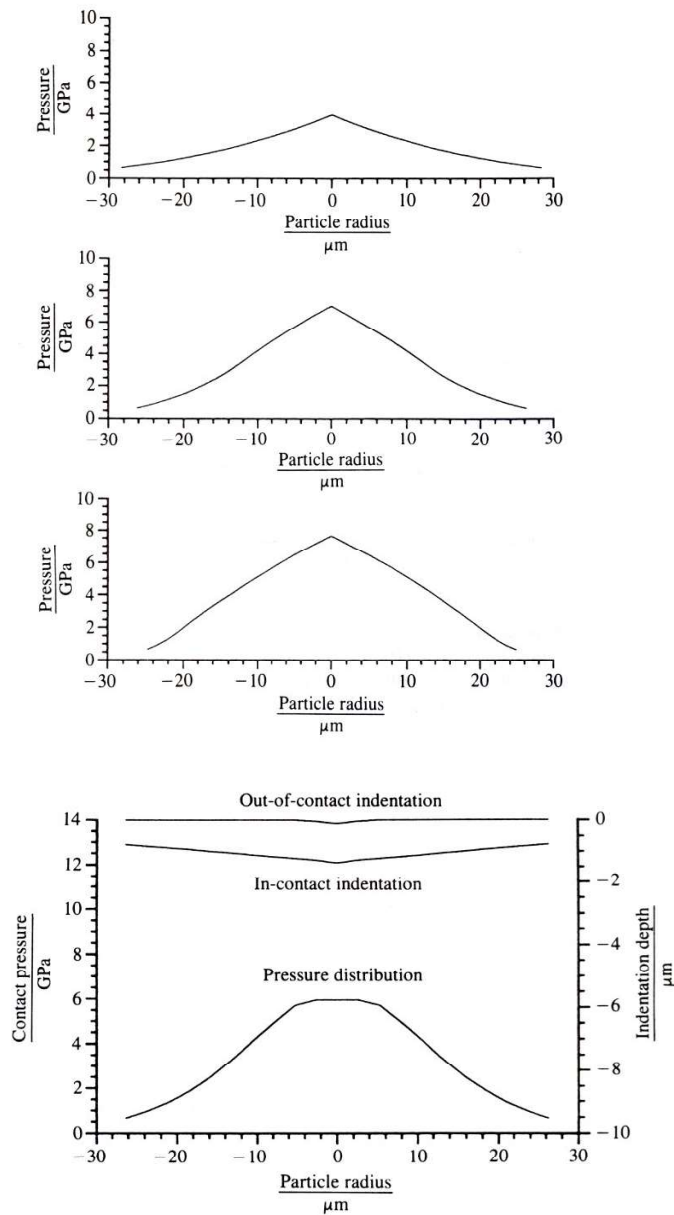
Figure 10. Contact pressure distributions on the left, calculated for a 20 μm, 200 HV particle, squashed between hard surfaces with a 1 μm separating film and interface friction coefficients of 0.05, 0.10 and 0.20 from top to bottom; the surfaces are assumed purely elastic. Example of contact pressure on the right using surface plasticity modelling. (From the work of Hamer et al. [14].)

Nikas' models [23,27] showed quite graphically that, upon its entrapment in a lubricated contact, a ductile, spherical particle sticks to the contact counterface with the higher friction coefficient immediately and enters the contact. As it is squashed between the converging counterfaces, it is extruded and expands laterally. The fluid forces on the particle are dominating at the very early stages of entrapment but are quickly overcome by the normal and frictional forces between the particle and the counterfaces. The crushing pressure on the particle rises as the particle is dragged towards the contact and is maximised when the particle enters the flat contact region known as the Hertzian zone. At the same time, the rapid plastic deformation of the particle and its shearing on the contact counterfaces owed to its extrusion and the sliding speed of the contact (if any) generate heat, which is partitioned between the particle and the counterfaces, and is maximised when the particle enters the Hertzian zone of the contact. Naturally, the amount of frictional heat depends on the material properties, level of pressures and speeds but it was shown that even small metallic particles (e.g. 10 μm) and several times softer than the contact counterfaces are generating enough heat to raise counterface temperature by hundreds of degrees Celsius. The heat is localised in the vicinity of a particle and penetrates the counterfaces, having disappeared at a depth equal to the radius of the extruded particle disc (up to 200 μm for typical particles). In a typical rolling-sliding contact such as in a rolling bearing, the time needed for a particle to pass through the contact is in the order of a few milliseconds or less. Calculation of the subsurface stress field by Nikas et al. [28] showed that the thermal stresses caused by the frictional heat are very high and often capable of causing plastic deformation to the counterfaces. Thus, Nikas called this type of damage "local scuffing" [27]. The theoretical analysis confirmed experimental results and speculations of Chandrasekaran et el. [19] regarding the effect of abrasive contaminants on scuffing, and extended the findings to cover not only hard particles but very soft ones as well.

Nikas' model of ductile debris deformation was subsequently extended in an attempt to verify earlier results and improve its precision and realism. In what was a very complex model, Nikas [29] advanced his modelling to include transient effects such as the thermoelastic displacement of the counterfaces in the vicinity of the particle, the lubricant pressure on the particle, convective heat losses from the particle and the counterfaces to the lubricant, internal heating along plastic shear zones inside the deforming particle, temperature dependency of mechanical and thermal properties of all bodies involved, thermal anisotropy of the counterfaces, a more precise heat partitioning between the particle and the counterfaces, etc. The advanced model not only confirmed earlier results on the level of frictional heating but actually predicted even higher temperatures, in the order of 1,000-2000 ºC and sometimes even more. As a result, thermal stressing is very high. In fact, thermal stresses are as much as ten times higher than the mechanical stresses on the particle, which means that ignoring frictional heating can give completely misleading results in terms of the risk of surface damage. The main conclusions of that work [29] were as follows.

(a) A soft, ductile particle becomes a flat, thin disc as it passes through a typical elastohydrodynamic contact.
(b) Upon entrapment, the particle sticks to the counterface with the higher friction coefficient, providing that the counterfaces are of equal hardness.
(c) The fluid forces on the particle are much weaker than the normal and frictional forces.

(d) The extrusion and shearing of the particle during its passage through an elastohydrodynamic contact result in frictional heating, which can be severe even for soft and small particles. The maximum flash temperature in the contact can reach hundreds of degrees Celsius and could, thus, cause tempering reactions and local scuffing. The maximum flash temperature is reached within 1 millisecond or less for typical cases, depending on the contact rolling and sliding speeds.

(e) The average contact pressure on the particle is maximized just before its entrance to the central (Hertzian) zone of the contact and this affects the location of the maximum flash temperature.

(f) Heat partition between the particle and the counterfaces is governed by the thermal properties of the affected bodies. Generally, the greatest amount of heat goes to the surface which the particle sticks to. Generally, the bigger and/or harder the particle, the smaller (as a percentage) the maximum temperature difference between the two counterfaces is. The biggest impact on the level of flash temperatures is caused by the size of the particle instead of its hardness. The maximum flash temperature difference between a 5 μm and a 20 μm particle of the same material is quite substantial (well over 1000 °C).

(g) Due to its plastic deformation in an elastohydrodynamic contact, a particle is a heat generator itself. The heat is generated inside the particle but accounts for only about 1% of the maximum flash temperatures encountered in the contact from the overall frictional heating.

(h) Convective heat losses from the particle and the counterfaces to the lubricant are negligible because of the small heat convection coefficient (as calculated for typical applications). The frictional heat transferred to the counterfaces is essentially conducted to their interior and is dissipated fast. It is found that the heat has dissipated completely at a depth equal to the semi-width of the Hertzian zone and, thus, deeper regions are not affected by the heat wave. Generally, the penetration depth of the frictional heat generated on the surface was found to be approximately equal to the radius of the particle-disc when fully deformed in the contact.

(i) The frictional heating produces thermal stresses, which in many areas are much greater than the mechanical stresses in the contact. Thermal stresses increase significantly the risk of damage, bringing the high-risk zone for plastic deformations very close to (or on) the surface.

(j) Following the particle's presence inside the contact, a hot spot is created on both counterfaces. Such hot-spots, if undergone plastic deformation, would sometimes appear as smooth and shiny indentations, the shiny (white-colour) appearance owing to the high heating followed by fast cooling to a much lower temperature. (There are characteristic similarities between these predictions and, for example, the experimental results of Zantopulos [101] on scuffing of tapered roller bearings, Tallian [102] (section 12.4 – case 4), and the experimental results of Ville et al. [15,16,103] on the appearance of dents caused by debris particles.)

(k) When plastically compressed in an elastohydrodynamic contact, soft and ductile particles are flattened and present a much larger interface for friction, as opposed to hard particles, which more-or-less retain their initial shape. Therefore, owing to the

domination of thermal stresses over mechanical stresses, soft particles can cause substantial damage and should never be seen as harmless.

(l) The creation of hot spots from the frictional heating of soft, ductile particles could explain some failures in concentrated contacts and resembles the damage characterized as "local scuffing".

(m) Because of the high heat core of the hot spots left behind squashed debris, it is sometimes expected to observe a secondary micro-cavity inside a dent (due to local material softening) and a matching hump on the centre of the bases of the deformed particle-discs.
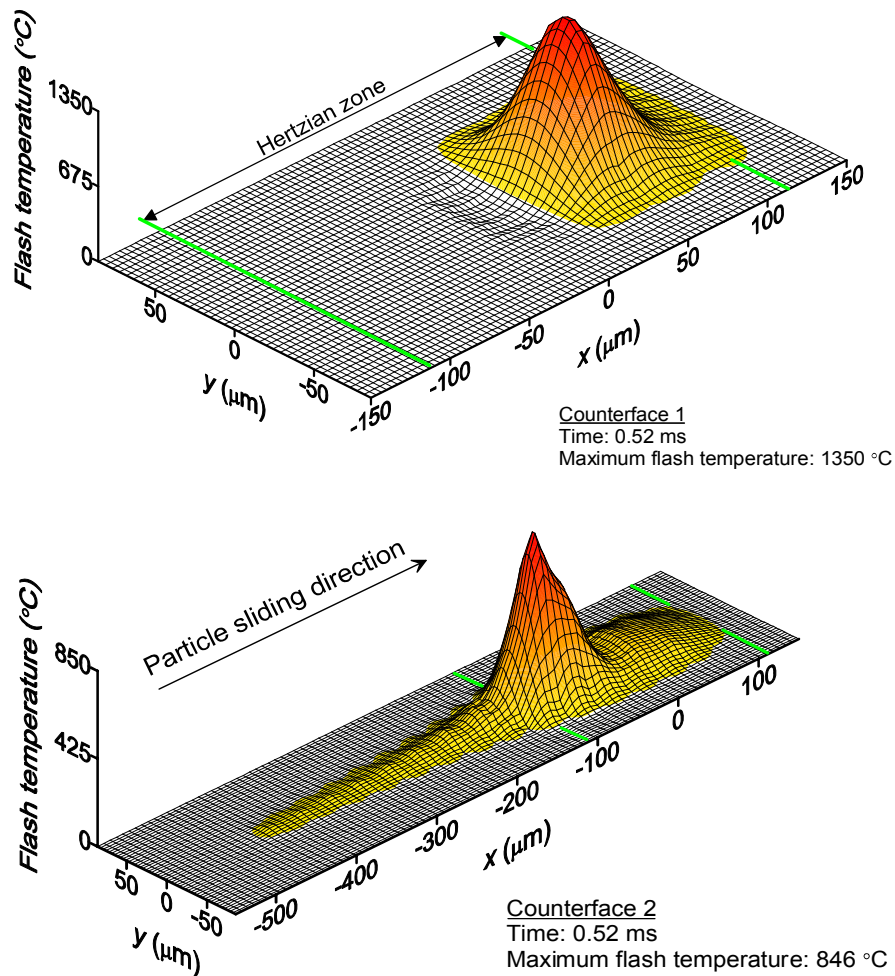
Figure 11. Flash temperature distributions on the counterfaces of a line, rolling-sliding, elastohydrodynamic contact, 0.52 milliseconds after trapping a 20 μm, 100 HV spherical, ductile particle. The particle is 8 times softer than the counterfaces. Sliding speed = 1 m/s; slide-roll ratio = 1. The particle sticks to counterface 1, which has a higher friction coefficient, and slides on counterface 2. At the instant shown, the particle starts exiting the Hertzian zone of the contact. (From the work of Nikas [25,29].)

Figure 11 shows an example of the flash temperature distributions on both counterfaces of a typical, rolling-sliding, elastohydrodynamic contact with central film thickness of 0.7 μm, squashing a 20 μm ductile particle that is 8 times softer than the counterfaces, taken from the work of Nikas [25,29]. Maximum flash temperature in excess of 1,300 °C is predicted as the particle, during its extrusion, sticks to the counterface with the higher friction coefficient and slides on the other. The contour maps of those temperature distributions are shown in Figure 12. Table 6 shows the results of the subsurface stresses for this example and it is clear that the thermal stresses are dominating the mechanical stresses (that is the stresses from particle squashing when frictional heating is ignored).
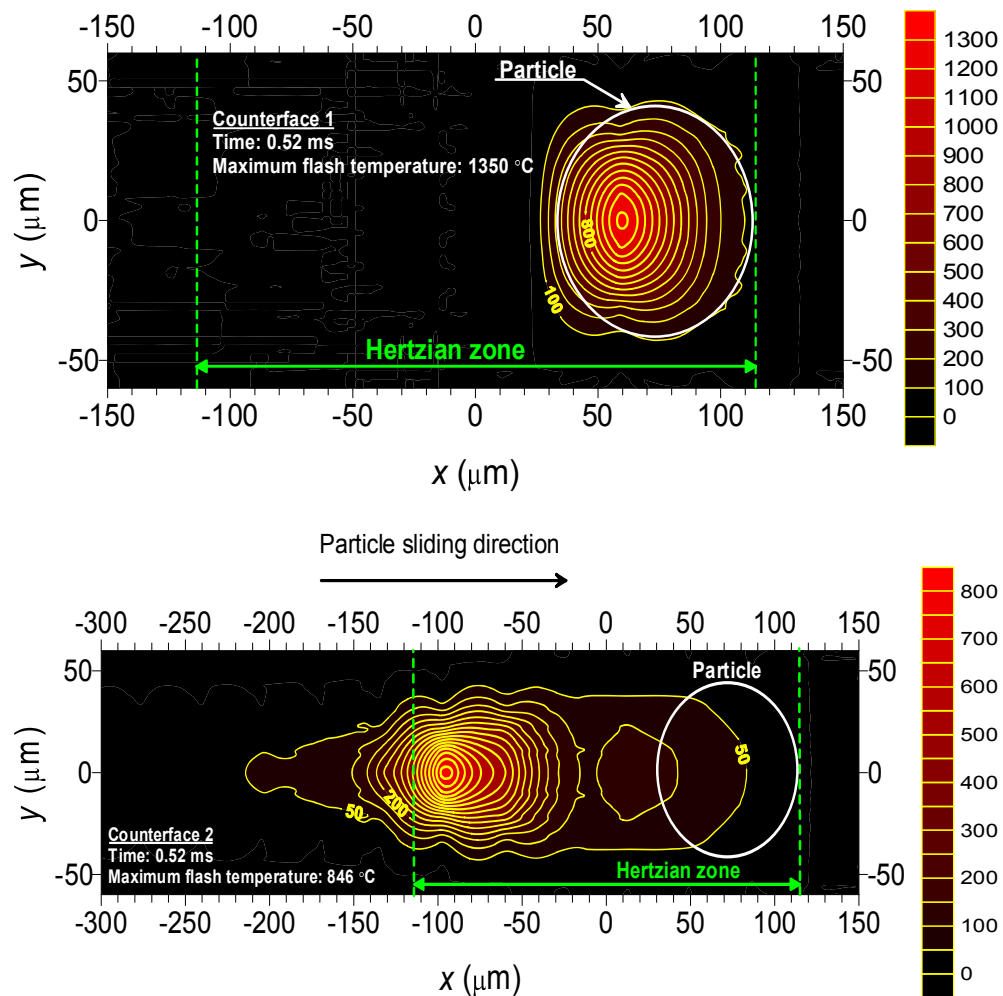
Figure 12. Contour maps of the flash temperature distributions shown in Figure 11. The particle sticks to counterface 1 and slides on counterface 2 (notice the hot trace left there). Temperatures shown are in degrees Celsius. (From the work of Nikas [25,29].)

Table 6. Overall (mechanical plus thermal) and thermal subsurface stress components
for the example of figures 11 and 12 (from the work of Nikas [25,29]).

Stress	Overall stress [GPa]		Thermal stress [GPa]	
	Body 1	Body 2	Body 1	Body 2
σ_{xx}	−5.75	−3.30	−5.29	−3.28
σ_{yy}	−5.23	−3.32	−5.27	−3.32
σ_{zz}	−7.22	−4.24	−6.74	−4.24
τ_{xy}	−0.07	+0.04	+0.07	−0.04
τ_{yz}	+1.00	+0.61	+1.04	+0.61
τ_{zx}	+0.29	−0.14	+0.25	+0.12

It is thus realised that thermal stresses increase the risk of surface damage in the contact significantly. Although the location of thermal stress maxima is, generally, different from the location of mechanical stress maxima, there are many areas where thermal stresses prevail. The strength of thermal stresses over mechanical stresses has been confirmed in several publications, for example Ju and Huang [104]. In an analytical study of thermal versus mechanical effects in high speed sliding surfaces, Marscher [105] speculated that strong compressive thermal loading could explain the occurrence of surface "mud-flat" cracks, which could promote and accelerate wear. Impressive results have also been obtained by Tseng and Burton [106] who wrote that "…*the thermal compressive stress is found to be ten times the normal load for the assumed contact conditions and hence it is this stress rather than simple load concentration which causes the trouble*". Moreover, an important aspect of thermal stresses in general is that they bring the high-risk strain zone closer to the surface [107,108], which explains the initiation and propagation of surface thermo-cracks and spalling in scuffed components.

Regarding debris particle heat generation, it may be difficult to comprehend that a flash temperature of more than 1000 °C can be reached in half a millisecond and caused by a small and soft particle. Nevertheless, similar results have been obtained in many publications and the interested reader is directed to the detailed discussions, additional analyses and related references contained in Nikas [25,29] on the theoretical and experimental validation of these results.

It is now clear that a squashed ductile particle is able to cause severe frictional heating, creating high thermal stresses. Even when the overall stress is below the yield limit of the contact counterfaces, the strong, localised heating can result in tempering reactions (for example martensite-to-austenite transformation at around 700-800 °C), which, followed by fast cooling, will introduce residual stresses and possibly initiate microscopic surface thermo-cracks. Such surface cracks can propagate fast, particularly when subjected to the high lubricant pressures met in elastohydrodynamic contacts.

Table 7 presents a flash-temperature parametric study [25,29]. As is clear in the table, a 20 μm spherical particle half as hard as the counterfaces (400 HV) is capable of causing a flash temperature rise of 1830 °C. For larger particles (e.g. 30 μm), the maximum theoretical temperatures can exceed 2,000 °C, the limitation being the softening of the particle and the yielding of the counterfaces. On the other side, small and very soft particles (e.g. 5 μm and 8

times softer than the counterfaces) do not cause *severe* frictional heating (table 7). It must also be emphasized that the results of table 7 were derived using friction coefficients of 0.20 and 0.15 for the two counterfaces, which are rather conservative. It is known that for temperatures higher than about 150 °C, the boundary lubricating film between the particle and a counterface is expected to melt and collapse. This would result in higher friction and, sometimes, the friction coefficient could even be doubled [109,110]. In such an occasion, the flash temperatures will be significantly higher because they very much depend on the friction coefficient.

Table 7. Theoretical maximum flash temperatures during ductile debris extrusion in a typical line, rolling-sliding, elastohydrodynamic contact. Counterface hardness is 800 HV. (Adapted from the work of Nikas [25,29].)

Particle diameter [μm]	Particle hardness [Vickers]	Maximum flash temperature [°C]	
		Surface 1	Surface 2
5	100	93	17
5	200	185	34
5	400	350	68
10	100	211	103
10	200	415	182
10	400	760	318
20	100	1350	846
20	200	1560	962
20	400	1830	1120

5.2. Brittle Particles

Samples from lubricant systems have shown that a large proportion of debris are ceramics and silicates [48]. Those are friable particles, which often fracture at the inlet zone of concentrated contacts and the fragments then readily enter the contacts. The damage to the contacts is then defined by the ultimate fragment size. In the case of tougher materials, surface indentation may be caused before particle fracture.

In a concentrated contact, low-toughness, brittle particles will fracture before the contact counterfaces yield (Figure 13(a); see also Figure 6(b)). The produced fragments enter the contact and, depending on their size, they may or may not be compressed. Eventually, all fragments are fractured below a critical size, depending on their original size, fracture toughness and counterface hardness. Surface damage may follow accordingly. On the other hand, brittle particles of high toughness may plastically deform the counterfaces prior to being fractured (Figure 13(b); see also Figure 6(c)). Upon further compression, those particles may fracture as well and, again, the fragments will enter the contact, possibly causing further damage, depending on their size, fracture toughness and counterface hardness.

In practise, almost all ceramic debris will cause damage to hardened steels [50]. Therefore, the important factor is the ultimate fragment size because this is what governs the magnitude of damage. The fracture of brittle materials is caused by the existence of flaws and subsequent propagation of such micro-cracks in the presence of a stress field. Tensile stresses

open the cracks and compressive stresses close them. Thus, brittle materials fail in tension. Based on this observation and using the Hertzian pressure for the contact of a sphere (simulated particle) on a flat surface and a simple equation from fracture mechanics, Dwyer-Joyce [49] derived an equation relating the critical flaw size, a_{cc}, to the fracture toughness, K_{IC}, and the counterface hardness, H, assuming that the maximum Hertzian pressure is equal to the counterface indentation hardness. Assuming that the particle diameter cannot be reduced below a_{cc}, the final fragment size is [49,51]:

$$\alpha_{cc} = \frac{1}{\pi}\left[\frac{3K_{IC}}{(1-2\nu)H}\right]^2 \tag{4}$$

where ν is the Poisson's ratio of the counterface. Table 8 shows a comparison of the predictions from Eq. (4) and the experimental results of Dwyer-Joyce [49] on some brittle debris. The agreement is reasonable.
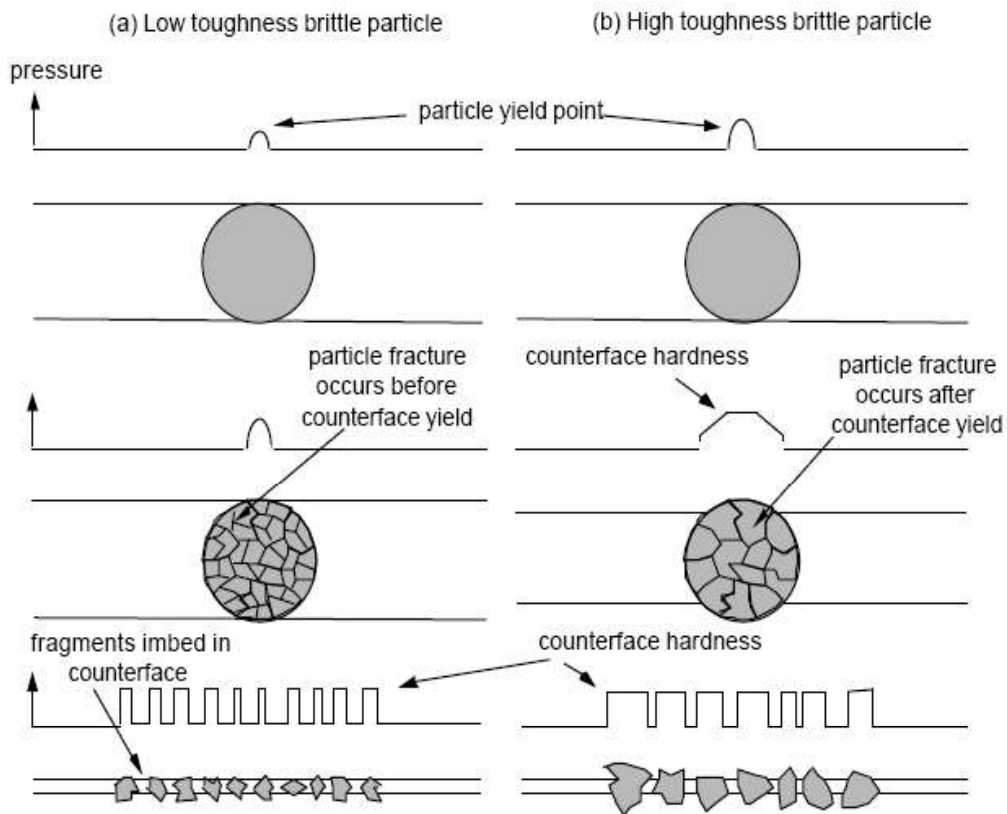
Figure 13. Behaviour of brittle particles during compression: (a) low toughness particle (left) and (b) high toughness particle (right). (From Dwyer-Joyce [49].)

Table 8. Comparison of ultimate fragment size between theory (Eq. (4)) and experiment (from Dwyer-Joyce [49]).

Material	Fracture toughness [MPa·m$^{1/2}$]	Ultimate fragment size (Eq. (4)) [μm]	Experimental fragment size [μm]
Quartz	0.5	0.1	
Glass	0.75	0.2	0.2-0.5
Arizona dust	1.5	0.7	0.2-0.9
Boron carbide	1.7	0.8	0.2-0.5
Alumina	3	2.6	2-3
Silicon carbide	4	4.7	5-10

5.3. Abrasive Wear

Abrasive wear of a surface from a debris particle occurs when the particle digs in, slides and ploughs out grooves of material on the surface (Figure 14). In 1957, Burwell [111] distinguished two kinds of abrasive wear, namely two-body and three-body abrasive wear. From the perspective of particle-caused abrasive wear, two-body wear occurs when a particle remains stuck or imbedded on one counterface of a concentrated contact and scratches the other. Alternatively (three-body wear), a particle may roll or tumble during the sliding motion of the counterfaces and, thus, cause a series of dents on one or both counterfaces.

When one counterface is softer than the other, experiments (see for example [4,8,9,49,51]) have shown that particles imbed the softer counterface and scratch the harder. However, when the softer surface is polished, the particles may scratch this surface, too [9]. These phenomena may be explained by the difference in the friction coefficients of the two surfaces, particularly when the ploughing component of friction and the role of surface roughness in raising the friction coefficient are taken into consideration. In fact, Nikas' theoretical modelling work [23,25,27,29] has shown that a ductile particle will stick to the counterface with the higher friction coefficient as soon as it is trapped. This means that, in many cases, the harder elements suffer from abrasion and the softer elements from indentation. This discovery is useful in establishing which element will fail first. For example, in a study of the abrasive wear of railway tracks by solid contaminants, Grieve et al. [11] found evidence that particles were embedding in the softer wheel and scratching the hard rail surface, causing the rail to wear 2.5 times faster than the wheel.

Another interesting observation concerns the effect of the lubricant film thickness and slide-roll ratio of a contact on the nature of debris-related abrasive wear. Particle rolling and tumbling in a lubricated contact depends on the solid pressure exerted on the particle as it passes through the contact. In a typical elliptical, elastohydrodynamic contact such as that of a ball in a groove, the thickness of the lubricating film has the characteristic "horseshoe" appearance (see the bottom part in Figure 15), which means that it is lower in the darker, horseshoe zone and has a central plateau. This may explain the experimental findings of, for example, Dwyer-Joyce [4,49], which indicate that particles are tumbling through the central zone of the contact and plough and roll over at the sides – see the top part of Figure 15. Some grooves appearing in the central zone may be owed to the larger particles in the abrasive size band [4]. The precise morphology of damage very much depends on the particle size to local

film thickness ratio. In fact, Williams and Hyncica [8] suggested that for tumbling to occur, the aforementioned ratio must be less than about 2. Naturally, the shape of the particles also plays an important role in particle tumbling and ploughing [112]; sharper particles are more likely to plough.
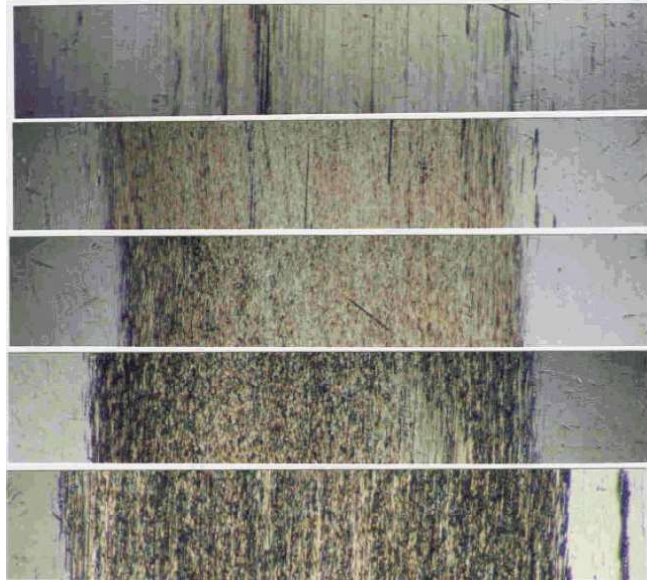
Figure 14. Photomicrograph (magnification = 100) of ball wear tracks from five tests with diamond abrasives of size bands 0-0.5 μm, 0.5-1.0 μm, 1-2 μm, 2-4 μm, and 3-6 μm. Film thickness = 0.4 μm, slide-roll ratio = 20%. (From Dwyer-Joyce [49].)
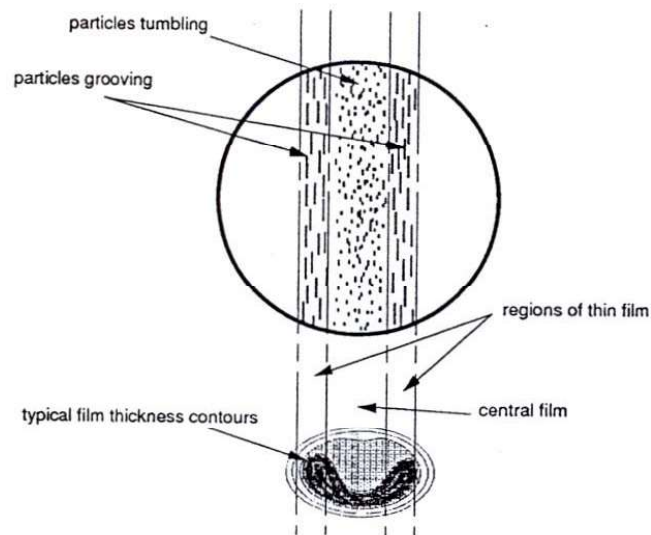
Figure 15. Ball wear pattern from ball-on-disc tests with 0.5-1.0 μm diamond abrasive powder; slide-roll ratio = 20%. (From Dwyer-Joyce [4,49].)

In predicting or calculating the wear from abrasive particles, the local surface velocities must be known and accounted for. Specifically, the magnitude of relative sliding between the contact counterfaces must be precisely known in order to estimate the distance a particle will slide and the length of the resulting wear track. This is characteristic in elliptical contacts, which exhibit the so-called "Heathcote slip" (see for example section 8.5 in Johnson [92]), a micro-slip occurring in the contact and attributed to the variable peripheral velocity of the counterfaces in the contact, owed to surface curvature and deformation. Experimental results show that abrasive wear from debris particles follows the Heathcote slip variation, that is, it is greater where the slip velocity is greater (see figures 16 and 17). Chao et al. [37] have speculated that soft, ductile particles, once deformed to sharp platelets, work-hardened and having re-entered a contact ellipse, may shear off surface material as they rotate or spin subjected to the Heathcote differential slip.
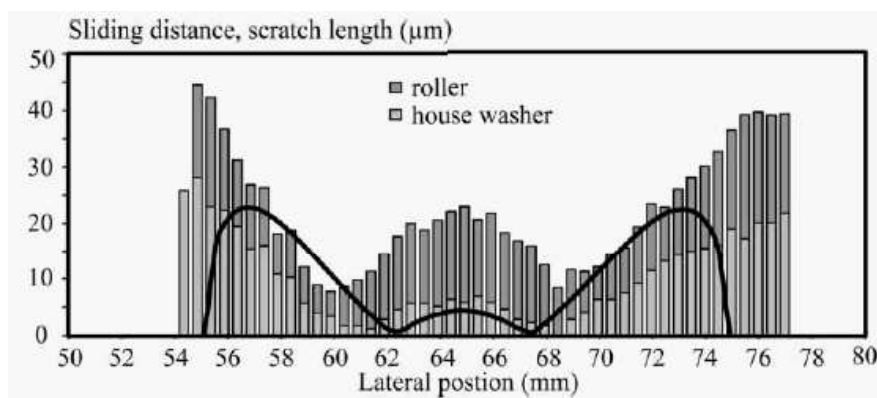
Figure 16. Scratch length for the roller and house washer in debris-related abrasive wear tests on spherical roller thrust bearings (from Nilsson et al. [12]).
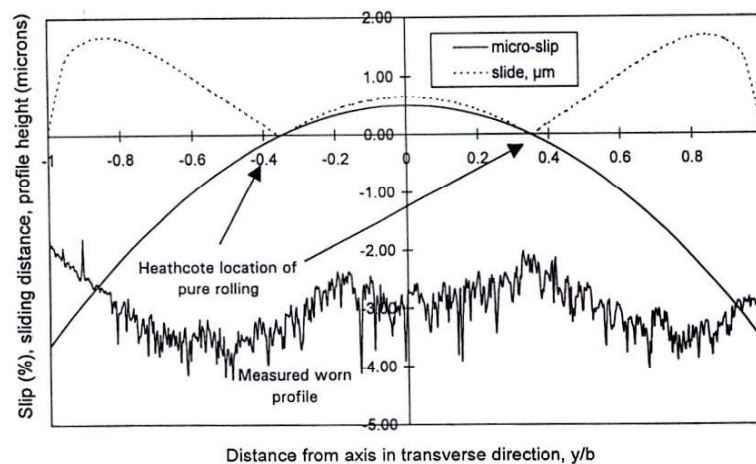
Figure 17. Worn inner raceway profile of a ball bearing (transverse direction) and micro-slip distribution. Notice that regions of greatest material removal correspond to those of increased sliding. (From Dwyer-Joyce [10].)

Concluding this introduction, it is noted that the literature on abrasive wear is very large, spanning many decades. Therefore, it is impossible to present a thorough discussion on this topic. For further information, interested readers are directed to references [4-12,49,71,72,74,76,77,112], the references quoted therein, as well as to books on tribology, particularly chapter 6 in Hutchings' book [69].

5.4. Fatigue Life of Debris Dented Surfaces

The detrimental effects of debris particles in lubricated contacts were presented and discussed in section 4. It was made clear that solid particles, both hard and soft, and both ductile and brittle or tough, are very often responsible for the damage observed on the counterfaces of machine element contacts, particularly those operating with thin lubricating films. Further results are presented in the present section on the effect of debris-caused indentations on contact fatigue, modelled theoretically and backed up by experimental studies.

The experimental and theoretical work of Sayles and Ioannides [47] in the 1980s revealed the critical factors causing a reduction of the fatigue life of debris-damaged rolling bearings. In summary, when surface dents are overrolled in elastohydrodynamic contacts, high pressure spikes appear at the edges of the dents or nearby, leading to stress concentration at or near the surface.
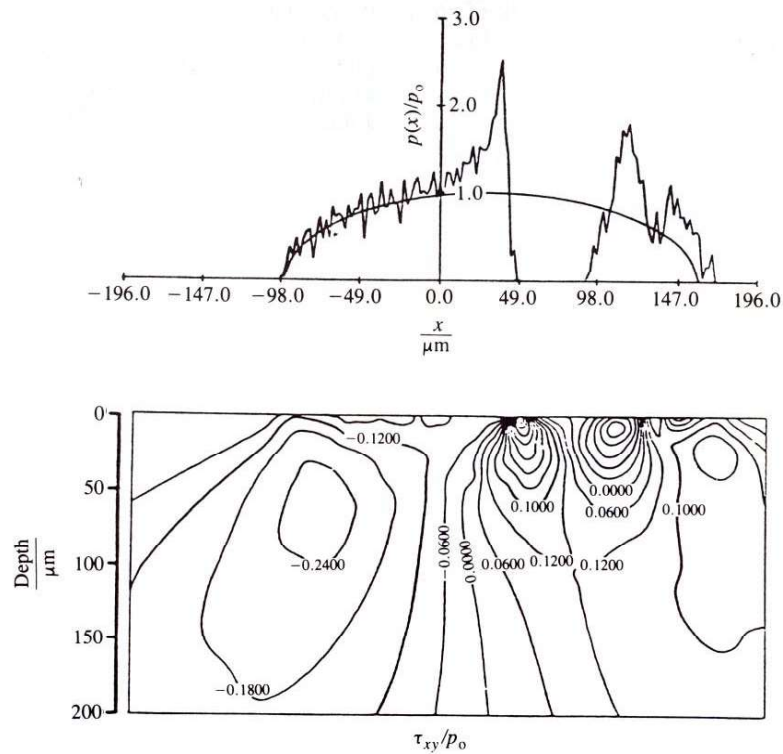
Figure 18. Theoretical, dry contact pressure (upper graph) and normalised subsurface shear stress τ_{xy} (lower graph) as a roller passes over a 50 μm diameter dent. (From Sayles and Ioannides [47].)

Figure 18 shows an example of a dry, line, rough contact with dent of about 50 μm in diameter. On the upper graph of Figure 18, the static contact pressure as the dent is overrolled has been plotted, based on a numerical solution of the related contact mechanics problem. The smooth line corresponds to the Hertzian pressure distribution in the absence of the dent and the spiky line corresponds to the contact pressure in the presence of the dent. It can be seen that the pressure spikes at the edges of the dent are in the order of 2.0-2.5 times the maximum Hertzian contact pressure.

The distribution of the subsurface shear stress τ_{xy} has been plotted on the lower graph of Figure 18. It is clear that, on the left part of the contact, which lies outside the dent, the shear stress distribution is smooth and close to that predicted by the Hertz theory [92]. On the right part though, the spiky contact pressure in the dent has altered the subsurface shear stress distribution significantly, causing stress concentrations to appear near the surface. This may then explain the origination and propagation of surface cracks after a number of overrollings or, equivalently, after a number of stress cycles.

An important factor in studying the effect of a dent on the fatigue life of a dented solid is the residual stress field created from the related plastic deformations in the area of the dent. Finite Element Analysis of surface indentations as for example by Ko and Ioannides [17], Lubrecht et al. [46], and Xu et al. [44] have shown that the subsurface stress field during the overrolling of a dent may be combined with the residual stress field from the plastic deformation that created the dent in the first place. Sayles and co-workers [34,48] quite early established that there is a difference between ductile and brittle particle indentations. Ductile-particle indentations are large and shallow; they are associated with a significant subsurface, tensile, residual stress build-up, which, when combined with the stress field from the normal overrolling of the dent, causes a significant reduction of the fatigue life. Brittle-particle dents on the other hand are smaller, with sharp, raised shoulders and associated residual stress fields much closer to the surface. As a result, the residual stresses of those dents are combined with the stresses from the normal overrolling of the dents and cause significant life reduction only in relatively lightly loaded contacts. Heavily loaded contacts with maximum subsurface stresses appearing deep below the surface are thus largely unaffected by brittle-particle induced dents [113].

Another important factor in evaluating the fatigue life reduction from surface indentations is the level of sliding and the direction of traction in a contact between dented surfaces. The direction of traction and the level of friction around a dent during its overrolling are clearly affecting the location of the maximum shear stress. This is important in predicting where around a dent a crack will originate. According to the experimental work of Ville and Nelias [38], the maximum shear stress is located ahead of the dent compared with the sliding direction if the dent is on the slower surface and behind the dent if the dent is on the faster surface. Similar results have been reported by Ville at al. [103].

In elastohydrodynamic contacts, the contact pressure during the overrolling of debris dents is governed by the Reynolds and elasticity equations, i.e. the effect of lubricant should be taken into account. The literature contains many theoretical studies where the elastohydrodynamic problem of a dented surface is numerically solved. For example, Xu et al. [43] used FEA results on the denting of a surface by a spherical indenter, which were subsequently used in a transient, thermal elastohydrodynamic, rolling-sliding, point-contact, numerical solver to analyse the dent effects on contact pressure, film thickness and

temperature profiles. They found that the dent, which exhibited a horseshoe-shaped material pile-up in the rolling direction, caused high pressure spikes when overrolled, associated with a corresponding film thinning. They also found that the temperature field was strongly affected by the dent and that the maximum temperature calculated was several times higher than that predicted in the absence of the dent. The pressure spikes caused by the dent resulted in high subsurface stresses and the maximum effective stress was brought closer to the surface, increasing the risk of spalling.

These results are experimentally verifiable [40]. Ville and Nelias [40] remark that the pressure peak and resulting stress concentration depends on the sliding direction. Specifically, it appears at the leading edge of the dent for driven surfaces and at the trailing edge for driving surfaces. Furthermore, the elastohydrodynamic effect depends on the actual condition of the lubricant in the dented contact and whether it is in a glassy state (owing to the very high pressure) or not. The present author speculates that the latter will influence how compliant or how good of an absorber the lubricating film is during the dynamic incident of dent overrolling.

Once a crack near a dent has originated in a lubricated contact, it might fill up with lubricant when overrolled, owing to capillary action and the high hydrodynamic pressure involved [114,115]. Thus, it has been speculated that the crack will open and propagate or shut as it is being overrolled, depending on the direction of traction. If the direction of traction is the same as the direction of contact motion (driver surface – see Figure 19), the crack is squeezed and shut before being overrolled. If, however, the direction of traction is opposite to the direction of contact motion (follower surface – see Figure 19), the crack lips are pulled apart and lubricant enters the crack via hydrodynamic pressurization, the described mechanism promoting the propagation of the crack [116-118].
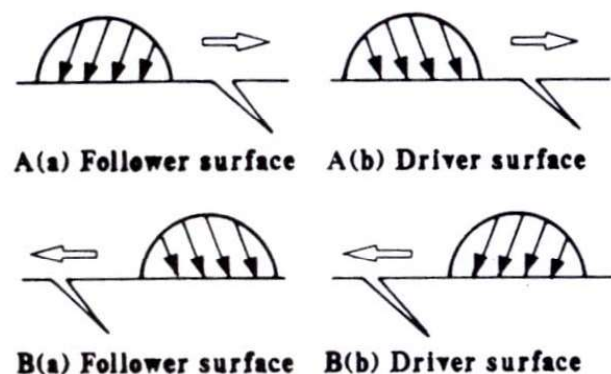
Figure 19. Inclined crack, direction of contact motion (thick arrow), and direction of traction (distributed arrows). (From Kaneta et al. [116].)

Returning to the issue of contact fatigue, if the residual stress field in the neighbourhood of a debris-induced dent is known and the subsurface stress field generated during the overrolling of the dent has been calculated, the calculation of the fatigue life of the damaged component can be attempted. This is based on several stress criteria, depending on the loading conditions. Moreover, several models have been developed to describe as accurately as possible what is, essentially, a stochastic process.

In this respect, the Ioannides-Harris fatigue life model [119], which improved upon the original Lundberg-Palmgren model [120,121] and is (at the time of writing) the industry standard in rolling bearings, has been used extensively in predicting the life expectancy of debris-dented surfaces [47]. According to that model, the stressed volume of material is subdivided in n elemental volumes ΔV_i. Then, the probability of survival, S, of the entire volume is calculated from

$$\ln\left(\frac{1}{S}\right) = N^e \sum_{i=1}^{n} A_i H\left(\sigma_i - \sigma_{ui}\right) \frac{\left(\sigma_i - \sigma_{ui}\right)^c}{Z_i^h} \Delta V_i \tag{5}$$

where N is the number of stress cycles, σ_i and σ_{ui} is the stress and the fatigue limit in a volume element, respectively, Z_i^h is a stress-weighted depth, H is the Heaviside step function, and A_i, e and c are application-dependent constants. It is obvious from Eq. (5) that because $H\left(\sigma_i - \sigma_{ui}\right) \neq 0$ only if $\sigma_i > \sigma_{ui}$, the summation is carried over only on volume elements with stress exceeding the local fatigue limit. Therefore, when the stress distribution is known in the neighbourhood of a dent, the reduction of fatigue life can be estimated by applying Eq. (5).

Similar probabilistic models have been developed by other researchers. For example, Tallian's exhaustive modelling work [30,45,122,123] has led to a combination of various models, not necessarily with direct physical justification, yet with reasonable agreement with experimental results. Ai [41,124] utilised the Weibull weakest-link theory to develop a life-reduction model due to debris denting. He found that fatigue life depends strongly on the indentation area density and slope, particularly for slopes exceeding 5°. It should also be emphasized that such models have satisfactory experimental verification and are backed-up by tedious, costly and time-consuming experimental work (see for example reference [125]). Detailed modelling work on the contact fatigue of dented surfaces has also been published recently by Antaluca and Nélias [94]. The interested reader is also directed to the review contained in section 6.4.1 of Roylance et al. [59].

5.5. Particle Entrainment and Entrapment in Concentrated Contacts

The processes of particle entrainment and entrapment in concentrated contacts determine the probability and nature of potential damage. If particles bypass a lubricated contact, they will obviously cause little or no damage at all. If they are trapped, they may cause surface abrasion, indentation, frictional heating, etc, depending on the surface speeds, film thickness and contact geometry. Thus, the experimental study and theoretical analysis of particle entrainment and entrapment is a vital step in understanding wear mechanisms and assessing the risks of damage.

The present author distinguishes particle entrainment and entrapment as follows: entrainment refers to particle transportation by a lubricant to a concentrated contact without the particle being squeezed by the contact counterfaces; entrapment refers to the process where the particle is in contact with both counterfaces and is elastically or plastically

compressed. Thus, entrainment precedes entrapment (without entrapment being guaranteed to happen).

The theoretical analysis of particles translating in viscous fluids is a Fluid Mechanics topic since at least the 19th century. In one of his pioneering theoretical studies, Stokes [126] in 1850 dealt with the translation of rigid spheres through unbounded, quiescent flows at low Reynolds number. The mathematical problem of particle translation and rotation in viscous fluids later received extensive treatment in some quite complex and long studies by Jeffery [127] in 1922 (dealing with ellipsoidal particles), Rubinow and Keller [128] in 1961 (formulating the transverse force on spinning spheres), Bretherton [129] in 1962 and Saffman [130] in 1965 (dealing with flows of low Reynolds number), Leal [131] in 1979 and [132] in [1980] (dealing with low Reynolds number flows and non-Newtonian fluids), Brunn [133-135] in 1976-77 (dealing with viscoelastic fluids and single or multiple translating and interacting spheres), Drew [136] in 1978 (dealing with particle forces in a slow flow), and Sugihara-Seki [137] in 1993 (dealing with a single elliptical cylindrical particle in channel flows at low Reynolds number). The aforementioned studies involve rigorous mathematical formulations of the forces acting on single or interacting, rigid particles, mainly in shear flows at low Reynolds number. They also contain long lists of references on the discussed topics, which help readers obtain an accurate picture of the problem and its mathematical treatment. In some cases, they even account for interactions among particles due to fluid disturbances and even electric forces, as in Saville [138]. Of general interest and practical value is also the study of Maxey and Riley [139], which deals with the equation of motion of a rigid particle in a nonuniform flow. However, from an engineering point of view, the formalism, generality and complexity of the previously mentioned studies is often impractical. Applied tribology usually requires simpler and more straightforward solutions or practical formulas.
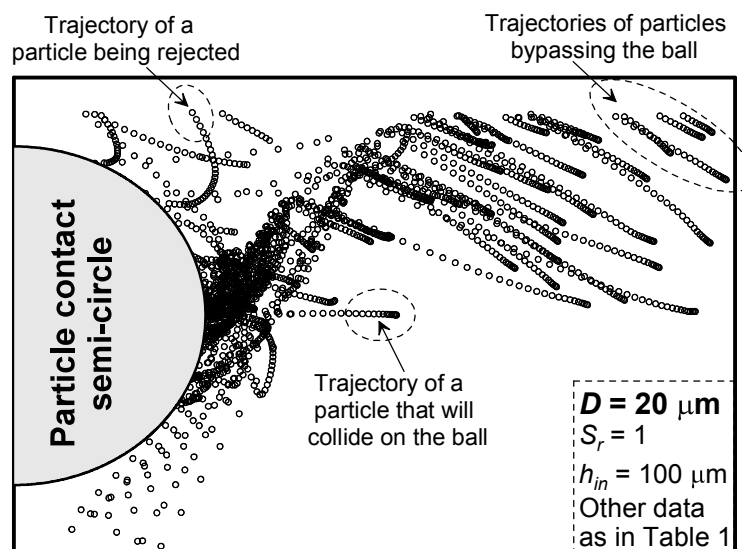
Figure 20. Theoretical simulation of particle entrainment in a lubricated contact (sphere rolling-sliding on a flat surface) with slide-roll ratio of 1 and oil bath thickness of 100 μm. The figure shows 30 possible trajectories of a 20 μm particle left at 30 randomly chosen positions in the flow in the upper half of the plot and in the inlet zone of the contact. (From Nikas [26].)

In this respect, Nikas [23,25,26] developed a model to study the entrainment of isolated spherical particles in the inlet zone of an elastohydrodynamic point contact of a sphere rolling-sliding on a flat surface. The analysis concerned particles larger than the minimum film thickness of the contact. The model was based on the solution of the Navier-Stokes equations for the viscous flow of a Newtonian fluid, followed by calculating the fluid drag force on a particle left at a random position in the inlet zone of the contact. Particle trajectories could thus be predicted for thousands of initial particle positions, creating a map of trajectories similar to that shown in Figure 20. The simulation showed how some particles were pushed away via the fluid back-flow and were swept aside the contact while others collided on the rolling element. The effects of the slide-roll ratio, the degree of lubricant starvation, the size and weight of a particle, and the oil viscosity on the risk of damage were examined and found to be significant (this is discussed later).

The next step in the analysis involves particle entrapment. A particle approaching a concentrated contact sees two surfaces converging (Figure 21). If the particle touches both counterfaces, normal reaction forces N_1, N_2 (see Figure 21), and tangential, frictional forces T_1, T_2 are exerted to it, in addition to the local fluid force $F^{(f)}$ from its interaction with the surrounding fluid. The resolution of all force components on the particle determines the direction the particle will follow and whether it will be entrapped or rejected.
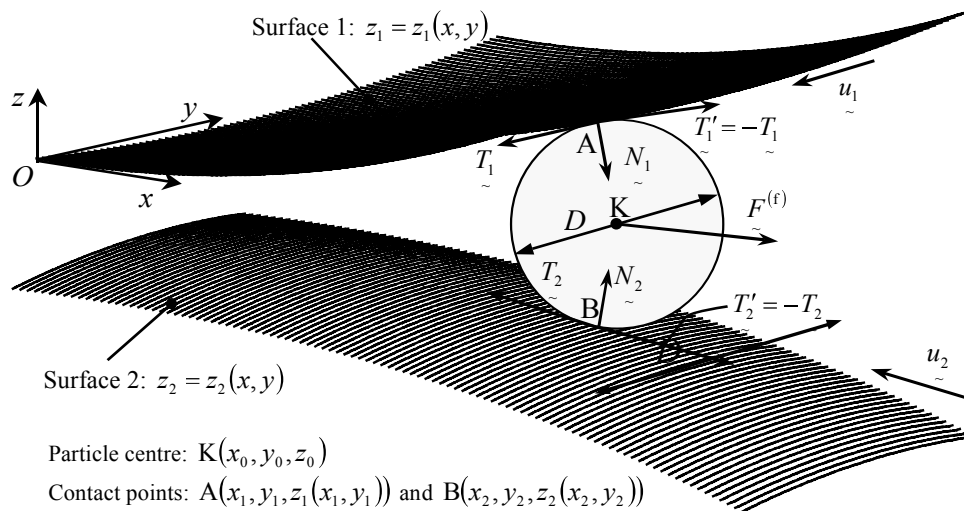
Figure 21. Spherical particle of diameter D in contact with the counterfaces of an elliptical, non-conforming contact, at points A and B. Surface speeds u_1 and u_2, particle fluid force $F^{(f)}$, particle-counterface reaction forces N_1 and N_2, and frictional forces T_1 and T_2 are depicted. (From Nikas [141].)

Elementary yet useful theoretical analyses of spherical particle entrapment can be found in references [10,35,49] for non-conforming, line contacts, and in reference [140] for a ball on a plane (still treated two-dimensionally, as in a line contact). In the aforementioned studies, simple equations were derived to determine whether a particle will be entrapped or rejected, and omit any fluid forces acting on the particle.

The present author analysed the problem of spherical-particle entrapment theoretically, both for line and for circular, non-conforming, rolling-sliding, elastohydrodynamic contacts [25,142], including particle-fluid interactions. For example, in reference [142] he derived the following equation for the fluid force on a spherical particle in the x-direction (Figure 21), which lies on the tangent plane of the contact:

$$F_{\text{fluid}}^{(x)} = 3\pi\eta\frac{u_1 + u_2}{2}\left[h_c - \frac{\pi}{4}\left(D - h_c\right)\right] \ (D > h_c) \tag{6}$$

where η is the fluid dynamic viscosity, u_1 and u_2 are the tangential velocities of the contact counterfaces, D is the particle diameter, and h_c is the central film thickness of the contact. The interesting property of Eq. (6) is that it shows that $F_{\text{fluid}}^{(x)} < 0$ (pushing the particle out of the contact) for $D > (1+4/\pi)h_c \cong 2.3 \times h_c$, which means that, in typical elastohydrodynamic contacts ($h_c < 1$ μm) and for all but the smallest particles, the fluid acts in favour of particle rejection from the contact.

Nikas [25,142] proceeded in deriving equations for all particle force components. His analysis showed that, as soon as the particle is entrapped, the normal and frictional forces on a particle greatly exceed the fluid forces and dominated the entrapment process. Only at the very beginning of particle entrapment the fluid forces play a significant role. Nikas also developed basic criteria for particle entrapment, based on the direction of the resultant particle force. As an example, Figure 22 shows the maximum particle diameter to enter a line contact for various typical parameters. Similar results were derived experimentally by Wan and Spikes [20] as well as by Cusano and Sliney [143].

In references [25,142], Nikas also derived particle force equations and entrapment criteria for circular, non-conforming, rolling-sliding, elastohydrodynamic contacts, including particle-fluid forces. He later extended those models to cover the general case of both conforming and non-conforming elliptical contacts in reference [141] and developed advanced particle entrapment criteria that introduced states other than the classical entrapment and rejection. The improved criteria include states such as "conditional entrapment", "weak rejection", "potential rejection", etc, and the classification is based on the direction of the various particle force components [141,144]. His analysis predict the exact behaviour of a spherical particle at the very early stage of its compression between the contact counterfaces of elliptical contacts and calculates both the maximum particle diameter for entrapment and the minimum particle diameter for unconditional rejection. This way, the effects of the contact geometry, load and speed, lubricant viscosity, and friction coefficients of the contact counterfaces were thoroughly examined for a wide range of operating conditions [144]. It was found that the friction coefficients play the major role in particle entrapment, followed by the contact load and speed, and, lastly, by the lubricant viscosity. The effects were, generally, non-linear and complex, yet supported by engineering experience.
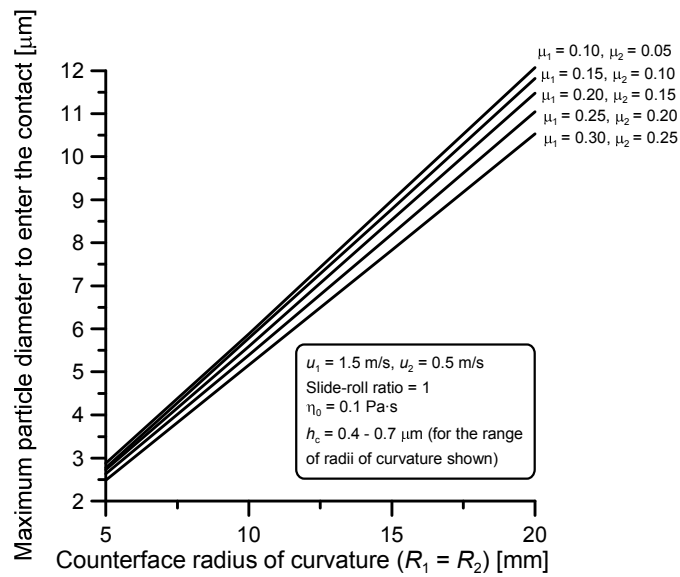
Figure 22. Maximum particle diameter to enter a line contact for various friction coefficients μ_1 and μ_2 of the contact counterfaces. (From Nikas [25,142].)
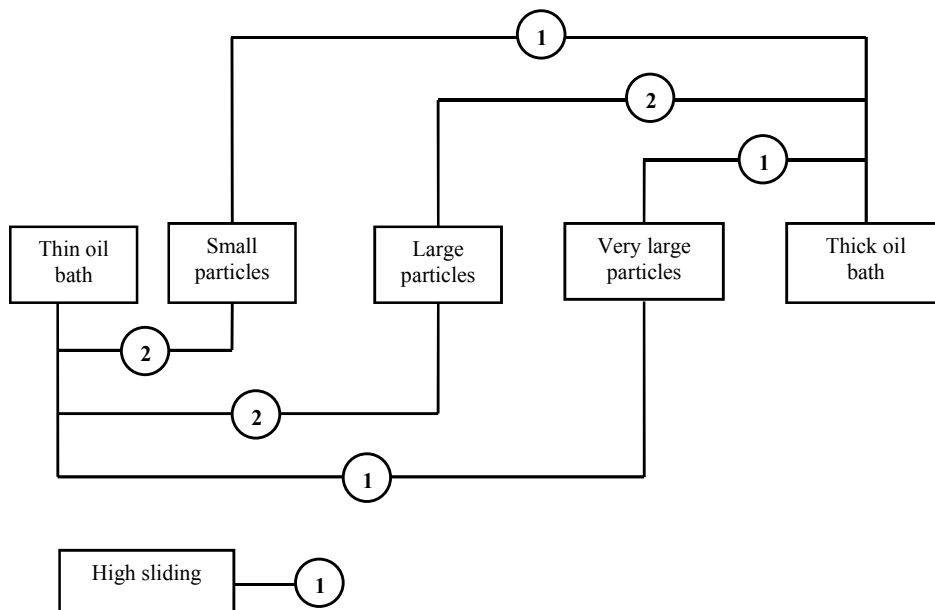
Definitions

$\boxed{1}$ Risk of particle agglomeration, fluid starvation, scuffing.

$\boxed{2}$ Risk of surface denting.

Figure 23. Schematic showing the risks of damage of a line contact, based on particle size, oil bath thickness and level of contact sliding velocity. (From Nikas et al. [23].)

Combining the analyses of particle entrainment and entrapment, Nikas et al. [23] created a schematic (Figure 23) showing the risks of damage of a line contact, based on particle size, oil bath thickness and level of contact sliding velocity. In creating such a risk analysis system, it is considered that particles that are difficult to be entrapped may obstruct the lubricant replenishment of a contact by accumulating at the inlet. The subsequent lubricant starvation of the contact could lead to film collapse and even scuffing. Such effects have been formulated and discussed in Nikas [23,25,26,141,142]; they have also been observed experimentally [20,22,145-148] using methods such as optical interferometry, high speed photomicrography, microscopy and video recording to observe real-time particle entry in point contacts. In fact, particle agglomeration has been observed by Oktay and Suh [148] in boundary lubricated, sliding contacts, and related to a rise in friction. Interestingly, wear particle accumulation in the inlet zone of lubricated contacts has been observed by Enthoven and Spikes [22], which led them to postulate that scuffing may be caused by a critical rate of wear debris production and accumulation of the debris in the inlet zone of a contact.

In a detailed theoretical analysis, Nikas [25,26] extended his previous model [23] on particle entrainment to point contacts and evaluated a number of risks for contact damage from debris particles. Based on a large number of theoretical simulations, he evaluated probabilities such as that of particle accumulation, particle entrapment, particle accumulation *and* entrapment (combined), particle-rolling-element collision, etc. The results were then gathered in a table (see table 9) showing which combinations of system operating parameters carry which damage risk.

Table 9. Combinations of operating conditions and parameters promoting various damage modes in a point contact (ball on plane). (Theoretical analysis from Nikas [23].)

Limits of this study: $5\,\mu m \le D < 50\,\mu m$; $50\,\mu m \le h_{in} \le 500\,\mu m$; $0.0 < S_r \le 2.0$	Risk of particle accumulation • Inlet blockage • Oil starvation • Film collapse • Scuffing		Risk of particle entrapment • Surface indentation • Abrasion				Overall risk of damage				
D — Smaller particles	(✓)						✓	✓			
D — Bigger particles		✓	✓	✓	✓	✓			✓	✓	✓ ✓
h_{in} — Starved contact			✓	✓			✓		✓	✓	
h_{in} — Flooded contact	✓	✓			✓	✓		✓			✓ ✓
S_r — $0.0 < S_r < 0.5$			✓		✓				✓		✓
S_r — $0.5 < S_r < 1.5$							✓	✓			
S_r — $1.5 < S_r < 2.0$	(✓)	✓		✓		✓				✓	✓

Example: the combination shown inside the dashed ellipse, namely ("smaller particles" + "flooded contact" + "$1.5 < S_r < 2.0$") carries the risk of particle accumulation. A combination is a triplet (D, h_{in}, S_r), where D is the particle diameter, h_{in} is the oil bath thickness and S_r is the slide-roll ratio.

In the case of a particle smaller than the minimum film thickness, theoretical studies have examined issues related to the disturbance created by the particle as it enters an elastohydrodynamic or hydrodynamic contact. For example, Kang et al. [149] modelled the entry of a rigid, ellipsoidal particle in a rolling-sliding elastohydrodynamic contact and showed that the particle creates a significant pressure build-up in its vicinity. This is associated with a change to the local film thickness. They also showed that the back flow of the contact plays a key role in particle entry. Languirand and Tichy [150] presented a study on the approximate solution of the Stokes equations to determine the effect of a two-dimensional, high aspect ratio particle of arbitrary cross-section on the pressure and velocity fields of a plane slider bearing. Their solution showed a pressure drop at the particle location, dependent on particle size, velocity and location. They also showed that the particle has a major effect on the bearing pressure field when it is able to obstruct the flow of lubricant. Experimental studies related to these phenomena have also been conducted, mainly to analyse the effectiveness of lubricant additives such as PTFE (polytetrafluoroethylene) (see for example reference [151]) or the behaviour of colloidal nanoparticles in thin film lubricated contacts (see for example reference [152]).

6. Conclusion

Debris particulates are responsible for a great number of failures of engineering components. Their minute size should never be underestimated. Understanding the mechanisms of debris-related damage in machine element contacts requires expertise but the fact remains that proper filtration is of paramount importance in avoiding premature failures and achieving the projected service life of engineering components. This chapter was introductory to the detrimental effects of debris. It did not discuss beneficial properties of some particles such as those used as solid lubricants and in powder and granular lubrication. The related topics are quite extensive and a proper discussion requires a separate chapter. The reader must keep in mind that lubricant cleanliness is truly one of the most important factors in achieving projected life expectancies of machine elements and having a machine that operates reliably for as long as it was designed for.

Acknowledgments

References

[1]   Kjer, T. *Wear*. 1981, 69, 395-396.
[2]   Leng, J. A.; Davies, J. E. *Wear*. 1988, 122, 115-119.

[3]   Leonardo da Vinci. *Codex Madrid I*. 1493, p. 119.

[4]   Dwyer-Joyce, R. S.; Sayles, R. S.; Ioannides, E. *Wear*. 1994, 175, 133-142.

[5]   Rabinowicz, E.; Mutis, A. *Wear*. 1965, 8, 381-390.

[6]   Richardson, R. C. D. *Wear*. 1968, 11, 245-275.

[7]   Xuan, J. L.; Hong, I. T.; Fitch, E. C. ASME *J. Tribol*. 1989, 111, 35-40.

[8]   Williams, J. A.; Hyncica, A. M. *J. Phys. D: Appl. Phys*. 1992, 25, A81-A90.

[9]   Hamilton, R. W.; Sayles, R. S.; Ioannides, E. *Proc. 24th Leeds-Lyon Symposium on Tribology, Elsevier Tribology and Interface Engineering Series*. 1998, 34, 87-93.

[10]   Dwyer-Joyce, R. S. *Wear*. 1999, 233-235, 692-701.

[11]   Grieve, D. G.; Dwyer-Joyce, R. S.; Beynon, J. H. *Proc. IMechE, Part F: J. Rail and Rapid Transit*. 2001, 215, 193-205.

[12]   Nilsson, R.; Dwyer-Joyce, R. S.; Olofsson, U. *Proc. IMechE, Part J: J. Eng. Tribol*. 2006, 220, 429-439.

[13]   Hamer, J. C.; Sayles, R. S.; Ioannides, E. *Proc. 14th Leeds-Lyon Symposium on Tribology, Elsevier Tribology and Interface Engineering Series*. 1987, 12, 201-208.

[14]   Hamer, J. C.; Sayles, R. S.; Ioannides, E. STLE *Tribol. Trans*. 1989, 32, 281-288.

[15]   Ville, F.; Nelias, D. *Proc. 24th Leeds-Lyon Symposium on Tribology, Elsevier Tribology and Interface Engineering Series*. 1998, 34, 399-409.

[16]   Ville, F.; Nelias, D. *STLE Tribol. Trans*. 1999, 42, 231-240.

[17]   Ko, C. N.; Ioannides, E. Debris denting – The associated residual stresses and their effect on the fatigue life of rolling bearings: An FEM analysis. *Tribological Design of Machine Elements* (Ed. D. Dowson, C. M. Taylor, M. Godet, and D. Berthe), Elsevier, Amsterdam, The Netherlands, 1989, 199-207.

[18]   Kang, Y. S.; Sadeghi, F.; Hoeprich, M. R. *ASME J. Tribol*. 2004, 126, 71-80.

[19]   Chandrasekaran, S.; Khemchandani, M. V.; Sharma, J. P. *Tribol. Intern*. 1985, 18, 219-222.

[20]   Wan, G. T. Y.; Spikes, H. A. *STLE Tribol. Trans*. 1987, 31, 12-21.

[21]   Khonsari, M. M.; Wang, S. H. *Wear*. 1990, 137, 51-62.

[22]   Enthoven, J. C.; Spikes, H. A. *Proc. 21st Leeds-Lyon Symposium on Tribology, Elsevier Tribology and Interface Engineering Series*. 1995, 30, 487-494.

[23]   Nikas, G. K.; Sayles, R. S.; Ioannides, E. *Proc. IMechE, Part J: J. Eng. Tribol*. 1998, 212, 333-343.

[24]   Khonsari, M. M.; Pascovici, M. D.; Kucinschi, B. V. *ASME J. Tribol*. 1999, 121, 90-96.

[25]   Nikas, G. K. *Theoretical modelling of the entrainment and thermomechanical effects of contamination particles in elastohydrodynamic contacts*. Ph.D. thesis, Imperial College London, Mech. Eng. Dept., London, England, 1999.

[26]   Nikas, G. K. *ASME J. Tribol*. 2002, 124, 461-467.

[27]   Nikas, G. K.; Ioannides, E.; Sayles, R. S. *ASME J. Tribol*. 1999, 121, 272-281.

[28]   Nikas, G. K.; Sayles, R. S.; Ioannides, E. *ASME J. Tribol*. 1999, 121, 265-271.

[29]   Nikas, G. K. *ASME J. Tribol.*, 2001, 123, 828-841.

[30]   Tallian, T. E. *ASME J. Lubr. Technol*. 1976, 384-392.

[31]   Loewenthal, S. H.; Moyer, D. W. *ASME J. Lubr. Technol*. 1979, 101, 171-176.

[32]   Ronen, A.; Malkin, S.; Loewy, K. *ASME J. Lubr. Technol*. 1980, 102, 452-458.

[33]   Loewenthal, S. H.; Moyer, D. W.; Needelman, W. M. *ASME J. Lubr. Technol*. 1982, 104, 283-291.

[34] Hamer, J. C.; Lubrecht, A. A.; Ioannides, E.; Sayles, R. S. *Proc. 15th Leeds-Lyon Symposium on Tribology*, *Elsevier Tribology and Interface Engineering Series*. 1989, 14, 189-197.

[35] Dwyer-Joyce, R. S.; Hamer, J. C.; Sayles, R. S.; Ioannides, E. *Proc. 18th Leeds-Lyon Symposium on Tribology*, *Elsevier Tribology and Interface Engineering Series*. 1992, 21, 57-63.

[36] Nixon, H. P.; Zantopulos, H. *STLE Lubr. Eng.* 1995, 51, 732-736.

[37] Chao, K. K.; Saba, C. S.; Centers, P. W. *STLE Tribol. Trans.* 1996, 39, 13-22.

[38] Ville, F.; Nelias, D. *STLE Tribol. Trans.* 1999, 42, 795-800.

[39] Kahlman, L.; Hutchings, I. M. *STLE Tribology Trans.* 1999, 42, 842-850.

[40] Nelias, D.; Ville, F. *ASME J. Tribol.* 2000, 122, 55-64.

[41] Ai, X. *Proc. IMechE, Part J: J. Eng. Tribol.* 2001, 215, 563-575.

[42] Nilsson, R.; Olofsson, U.; Sundvall, K. *Tribol. Intern.* 2005, 38, 145-150.

[43] Xu, G.; Sadeghi, F.; Cogdell, J. D. *ASME J. Tribol.* 1997, 119, 579-587.

[44] Xu, G.; Sadeghi, F.; Hoeprich, M. *STLE Tribol. Trans.* 1997, 40, 613-620.

[45] Tallian, T. E. *ASME J. Lubr. Technol.* 1976, 251-257.

[46] Lubrecht, A. A.; Dwyer-Joyce, R. S.; Ioannides, E. *Proc. 18th Leeds-Lyon Symposium on Tribology*, *Elsevier Tribology and Interface Engineering Series*. 1992, 21, 173-181.

[47] Sayles, R. S.; Ioannides, E. *ASME J. Tribology*, 1988, 110, 26-31.

[48] Sayles, R. S.; Hamer, J. C.; Ioannides, E. *Proc. IMechE, Part G: J. Aerospace Eng.* 1990, 204, 29-36.

[49] Dwyer-Joyce, R. S. *The effects of lubricant contamination on rolling bearing performance*. Ph.D. thesis, Imperial College London, Mechanical Engineering Department, London, England, 1993.

[50] Sayles, R. S. *Proc. IMechE, Part J: J. Eng. Tribol.* 1995, 209, 149-172.

[51] Dwyer-Joyce, R. S. *Proc. 31st Leeds-Lyon Symposium on Tribology, Elsevier Tribology and Interface Engineering Series*. 2005, 48, 681-690.

[52] SKF Maintenance Products B.V. *Oil Cleanliness Control Course*. Seminar that took place from 9-9-1991 to 13-9-1991 in SKF-ERC (The Netherlands).

[53] Khonsari, M. M.; Booser, E. R. *Proc. IMechE, Part J: J. Eng. Tribol.* 2006, 220, 419-428.

[54] Barwell, F. T. *Proc. 10th Leeds-Lyon Symposium on Tribology (1983)*, paper I(i), pp. 3-10, Butterworth, 1984.

[55] Rigney, D. A. *Proc. 18th Leeds-Lyon Symposium on Tribology (1991)*, pp. 405-412; Elsevier, 1992.

[56] Roylance, B. J.; Albidewi, I. A.; Laghari, M. S.; Luxmoore, A. R.; Deravi, F. *Lubr. Eng.* 1994, 50, 111-116.

[57] Trevor, M. H. *Wear Debris Analysis and Particle Detection in Liquids*. English edition; Kluwer Academic Publishers, 1993.

[58] Kowandy, C.; Richard, C.; Chen, Y.-M.; Tessier, J.-J. *Wear*. 2007, 262, 996-1006.

[59] Roylance, B. J.; Williams, J. A.; Dwyer-Joyce, R. *Proc. IMechE, Part J: J. Eng. Tribol.* 2000, 214, 79-105.

[60] Stachowiak, G. W. *Tribol. Intern.* 1998, 31, 139-157.

[61] Roylance, B. J.; Raadnui, S. *Wear*. 1994, 175, 115-121.

[62] Raadnui, S.; Roylance, B. J. *Lubr. Eng.* 1995, 51, 432-437.

[63] Peng, Z.; Kirk, T. B. *Wear*. 1999, 225-229, 1238-1247.

[64] Bowen, E. R.; Westcott, V. C. *Wear particle atlas.* Final report to Naval Engineering Centre, Lakehurst, New Jersey, USA, Contract NO156-74-C-182, 1976.

[65] Anderson, D. P. *Wear particle atlas, revised.* Report NAEC-92.163, Naval Army engineering Centre, USA, 1982.

[66] Stachowiak, G. P.; Podsiadlo, P.; Stachowiak, G. W. *Tribol. Letters.* 2006, 24, 15-26.

[67] Beghini, E.; Dwyer-Joyce, R. S.; Ioannides, E.; Jacobson, B. O.; Lubrecht, A. A.; Tripp, J. H. *J. Physics D: Appl. Physics*, 1992, 25, 379-383.

[68] Eleftherakis, J. G.; Khalil, A. SAE Technical paper No. 900561, SAE International, USA, 1990.

[69] Hutchings, I. M. *TRIBOLOGY – Friction and Wear of Engineering Materials.* Butterworth-Heinemann, Oxford, UK, 1992 (reprinted in 2001).

[70] Sasaki, A. *Proc. IMechE, Part J: J. Eng. Tribol.* 2006, 220, 471-478.

[71] McKee, S. A. *SAE Trans*. 1927, 22, 73-77.

[72] Roach, A. E. *ASME Trans*. 1951, 73, 677-686.

[73] Rylander, H. G. *Mech. Eng.* 1952, 74, 963-966.

[74] Broeder, J. J.; Heijnekamp, J. W. *Proc. IMechE.* 1965-66, 180, 21-31.

[75] Fitzsimmons, B.; Clevenger, H. D. *ASLE Trans*. 1977, 20, 97-107.

[76] Ronen, A.; Malkin, S. *Wear*. 1981, 68, 371-389.

[77] Ronen, A.; Malkin, S. *J. Lubr. Technol.* 1983, 105, 559-569.

[78] General Motors Corporation. *New Departure Handbook* (7th edition), USA, 1971.

[79] Okamoto, J.; Fujita, K.; Toshioka, T. *J. of the Mechanical Engineering Laboratory (Tokyo)*, 1972, 26, 228-238 (NASA technical translation; NASA TT F-15, 653; June 1974).

[80] Dalal, H.; Cotellesse, G.; Morrison, F.; Ninos, N. *Final report on progression of surface damage in rolling contact fatigue.* SKF-AL74T002, SKF Industries Inc., February 1974. (AD-780453.)

[81] Wedeven, L. D. *Diagnostics of wear in aeronautical systems.* NASA TM-79185, 1979.

[82] Cunningham, J. S.; Morgan, M. A. *ASLE Lubr. Eng.* 1979, 35, 435-441.

[83] Bachu, R. S. *The influence of debris on rolling fatigue life.* Ph.D. thesis, University of London, England, 1980.

[84] Sayles, R. S.; Macpherson, P. B. *ASTM STP 771*. 1982, 255-275.

[85] Webster, M. N.; Ioannides, E.; Sayles, R. S. *Proc. 12th Leeds-Lyon Symposium on Tribology (1985)*, paper VIII(iii), 207-221; Butterworth, 1986.

[86] SKF General Catalogue. Catalogue 5000 E. June 2003.

[87] Akagaki, T.; Nakamura, M.; Monzen, T.; Kawabata, M. *Proc. IMechE, Part J: J. Eng. Tribol.* 2006, 220, 447-453.

[88] Miettinen, J.; Andersson, P. *Tribol. Intern*. 2000, 33, 777-787.

[89] Sari, M. R.; Haiahem, A.; Flamand, L. *Tribol. Letters*. 2007, 27, 119-126.

[90] Mizuhara, K.; Tomimoto, M.; Yamamoto, T. *Tribol. Trans*. 2000, 43, 51-56.

[91] Tomimoto, M.; Mizuhara, K.; Yamamoto, T. *Tribol. Trans*. 2002, 45, 47-54.

[92] Johnson, K. L. *Contact Mechanics*. Cambridge University Press, England, 1985.

[93] Hamer, J. C.; Hutchinson, J. *Denting of rolling element bearings by third body particles.* PCS report for SKF. Imperial College London, Mechanical Engineering Department, Tribology Group; England, 1992.

[94] Antaluca, E.; Nélias, D. *Tribol. Letters*. 2008, 29, 139-153.

[95] Blok, H. *Proc. IMechE, General Discussion on Lubrication*, London, 1937, 2, 222-235.

[96] Carslaw, H. S.; Jaeger, J. C. *Conduction of Heat in Solids* (second edition, 1957). Oxford University Press, England, (reprint 1993).

[97] Barber, J. R. *Int. J. Heat and Mass Transfer*. 1970, 13, 857-868.

[98] Hou, Z.-B.; Komanduri, R. *ASME J. Tribol.* 1998, 120, 645-651.

[99] Hou, Z.-B.; Komanduri, R. *ASME J. Tribol.* 1998, 120, 652-659.

[100] Hou, Z.-B.; Komanduri, R. *ASME J. Tribol.* 1998, 120, 660-667.

[101] Zantopulos, H. *ASME J. Tribol.* 1998, 120, 427-435.

[102] Tallian, T. E. *Failure Atlas for Hertz Contact Machine Elements*. ASME Press, New York, USA, 1992.

[103] Ville, F.; Coulon, S.; Lubrecht, A. A. *Proc. IMechE, Part J: J. Eng. Tribol.* 2006, 220, 441-445.

[104] Ju, F. D.; Huang, J. H. *Wear*. 1982, 79, 107-118.

[105] Marscher, W. D. *Wear*. 1982, 79, 129-143.

[106] Tseng, M.-L.; Burton, R. *Wear*. 1982, 79, 1-9.

[107] Roylance, B. J.; Siu, S. W.; Vaughan, D. A. *Proc. 12th Leeds-Lyon Symposium on Tribology (1985), Mechanisms and Surface Distress*. Butterworth, 1986, pp. 117-127.

[108] Ting, B.-Y.; Winer, W. O. *ASME J. of Tribol.* 1989, 111, 315-322.

[109] Russell, J. A.; Campbell, W. E.; Burton, R. A.; Ku, P. M. *ASLE Trans.* 1965, 8, 48-58.

[110] Lai, W. T.; Cheng, H. S. *ASLE Trans.* 1985, 28, 303-312.

[111] Burwell, J. T. *Wear*. 1957, 1, 119-141.

[112] Fang, L.; Kong, X.; Zhou, Q. *Wear*. 1992, 159, 115-120.

[113] Dwyer-Joyce, R. S.; Hamer, J. C.; Sayles, R. S.; Ioannides, E. *Proc. IMechE, Symposium titled "Rolling Element Bearings – Towards the 21st Century"*, pp. 1-8, London, England, 1990.

[114] Way, S. *J. Applied Mechanics*. 1935, 2, 49-58.

[115] Bower, A. F. *ASME J. Tribol.* 1988, 110, 704-711.

[116] Kaneta, M.; Yatsuzuka, H.; Murakami, Y. *ASLE Trans.* 1985, 28, 407-414.

[117] Murakami, Y.; Kaneta, M.; Yatsusuka, H. *ASLE Trans.* 1985, 28, 60-68.

[118] Kaneta, M.; Suetsugu, M.; Murakami, Y. *ASME J. Appl. Mechanics*. 1986, 53, 354-360.

[119] Ioannides, E.; Harris, T. A. *ASME J. Tribol.* 1985, 107, 367-377.

[120] Lundberg, G.; Palmgren, A. *Acta Polytechnica, Mech. Eng. Series*. Royal Swedish Academy of Engineering Sciences, 1947, 1, 7.

[121] Lundberg, G.; Palmgren, A. *Acta Polytechnica, Mech. Eng. Series*. Royal Swedish Academy of Engineering Sciences, 1952, 2, 96.

[122] Tallian, T. E. *ASME J. Tribol.* 1992, 114, 207-213.

[123] Tallian, T. E. *ASME J. Tribol.* 1992, 114, 214-222.

[124] Ai, X.; Nixon, H. P. *Tribol. Trans.* 2000, 43, 197-204.

[125] Lubrecht, A. A.; Venner, C. H.; Lane, S.; Jacobson, B.; Ioannides, E. Surface damage – Comparison of theoretical and experimental endurance lives of rolling bearings. *Proc. of Japan International Tribology Conference*, Nagoya, Japan, 1990.

[126] Stokes, G. G. *Proc. Cambridge Philosophical Society*. 1850, 1, 104-106.

[127] Jeffery, G. B. *Proc. Royal Soc. London A*. 1922, 102, 161-179.

[128] Rubinow, S. I.; Keller, J. B. *J. Fluid Mech.* 1961, 11, 447-459.

[129] Bretherton, F. P. *J. Fluid Mech.* 1962, 14, 284-304.

[130] Saffman, P. G. *J. Fluid Mech.* 1965, 22, 385-400.

[131] Leal, L. G. *J. Non-Newtonian Fluid Mech.* 1979, 5, 33-78.
[132] Leal, L. G. *Annual Review on Fluid Mech.* 1980, 12, 435-476.
[133] Brunn, P. *Rheologica Acta.* 1976, 15, 163-171.
[134] Brunn, P. *Rheologica Acta.* 1976, 15, 589-611.
[135] Brunn, P. *Rheologica Acta.* 1977, 16, 461-475.
[136] Drew, D. A. *J. Fluid Mech.* 1978, 88, 393-400.
[137] Sugihara-Seki, M. *J. Fluid Mech.* 1993, 257, 575-596.
[138] Saville, D. A. *Annual Review on Fluid Mech.* 1977, 9, 321-337.
[139] Maxey, M. R.; Riley, J. J. *Physics of Fluids.* 1983, 26, 883-889.
[140] Kusano, Y.; Hutchings, I. M. *Proc. IMechE, Part J: J. Eng. Tribol.* 2003, 217, 427-433.
[141] Nikas, G. K. *Proc. IMechE, Part J: J. Eng. Tribol.* 2006, 220, 507-522.
[142] Nikas, G. K. *ASME J. Tribol.* 2001, 123, 83-93.
[143] Cusano, C.; Sliney, H. E. *ASLE Trans.* 1982, 25, 183-189.
[144] Nikas, G. K. *Proc. IMechE, Part J: J. Eng. Tribol.* 2007, 221, 727-741.
[145] Dwyer-Joyce, R. S.; Heymer, J. *Proc. 22nd Leeds-Lyon Symposium on Tribology, Elsevier Tribology and Interface Engineering Series.* 1996, 31, 135-140.
[146] Cann, P. M. E.; Hamer, J. C.; Sayles, R. S.; Spikes, H. A.; Ioannides, E. *Proc. 22nd Leeds-Lyon Symposium on Tribology, Elsevier Tribology and Interface Engineering Series.* 1996, 31, 127-134.
[147] Wan, G. T. Y.; Spikes, H. A. *Proc. 12th Leeds-Lyon Symposium on Tribology (Mechanisms and Surface Distress)*, paper X(i), Butterworth, 1986.
[148] Oktay, S. T.; Suh, N. P. *Proc. 18th Leeds-Lyon Symposium on Tribology (Wear Particles), Tribology Series 21.* Elsevier, 1992, pp. 347-356.
[149] Kang, Y. S.; Sadeghi, F.; Ai, X. *ASME J. Tribol.* 2000, 122, 711-720.
[150] Languirand, M. T.; Tichy, J. A. *ASME J. Lubr. Technol.* 1983, 105, 396-404.
[151] Palios, S.; Cann, P. M.; Spikes, H. A. *Proc. 22nd Leeds-Lyon Symposium on Tribology, Tribology Series 31.* Elsevier, 1996, pp. 141-152.
[152] Chiñas-Castillo, F.; Spikes, H. A. *Proc. 26th Leeds-Lyon Symposium on Tribology, Tribology Series 38.* Elsevier, 2000, pp. 719-731.